Chem. Erde **62** (2002), 89–121
Urban & Fischer Verlag
http://www.urbanfischer.de/journals/chemerd

CHEMIE der ERDE
GEOCHEMISTRY

INVITED REVIEW

The Near Earth Asteroid Rendezvous Mission to Asteroid 433 Eros: A Milestone in the Study of Asteroids and their Relationship to Meteorites

Timothy J. McCoy[1], Mark S. Robinson[2], Larry R. Nittler[3] and Thomas H. Burbine[1]

[1]Department of Mineral Sciences, National Museum of Natural History, Smithsonian Institution, Washington DC, USA
[2]Department of Geological Sciences, Northwestern University, Evanston IL, USA
[3]Department of Terrestrial Magnetism, Carnegie Institution of Washington, Washington DC, USA

Received: 28. 3. 2002 · Accepted: 11. 4. 2002

Abstract

A milestone in the study of asteroids occurred on 14 Feb 2000, when the NEAR spacecraft entered orbit around the asteroid 433 Eros for a year of detailed observation of the geology, mineralogy and chemistry of the surface, before landing on the surface on 12 Feb 2001 and conducting the first science on the surface of a small Solar System body. This paper reviews the scientific results of THE NEAR MISSION. Eros is irregularly shaped, can be described by a best fit ellipse measuring 35 by 10.2 by 10.2 km, with a complex surface that includes a global regolith, asymmetrically distributed population of boulders, heavily cratered surface at diameters above 200 m, and grooves and ridges thought to record broad scale tectonic deformation. Significant albedo differences are associated with steeply sloping surfaces, indicating downslope movement of "relatively dark" regolith, leaving behind "fresher," "less-altered" material. The spectrally-derived mineral compositions and olivine: pyroxene ratio, absence of a global magnetic field, and the Mg/Si, Al/Si and Ca/Si ratios and K concentrations point to a primitive, chondritic

*** Corresponding address:**
Timothy J. McCoy, Department of Mineral Sciences, National Museum of Natural History, Smithsonian Institution, Washington, DC 20560-0119 USA
Tel.: ++1-202-357-2251; Fax: ++1-202-357-2476; e-mail: Mccoy.Tim@NMNH.SI.EDU

0009–2819/02/62/02-089 $ 15.00/0

body (most likely an ordinary chondrite), while a strong apparently-global depletion in sulfur and lower Fe/Si and Fe/O ratios at the landing site relative to ordinary chondrites are likely due to metal and sulfide migration due to partial melting throughout the entire asteroid or, more likely, through processing of the regolith layer by micrometeorite bombardment, sputtering and/or size/density segregations. Synthesis of the spectral and chemical data suggest the most likely meteoritic analog is either an ordinary chondritic composition that experienced alteration at the surface or less likely a primitive achondrite formed from an ordinary chondritic precursor. The markedly different compositions from the X-ray and gamma-ray experiments can be reconciled with a common silicate mineralogy through variable abundances of metal and/or sulfide. As we begin our detailed exploration of the diverse group of small bodies that make up the asteroid belt, NEAR has provided both a technical and scientific blueprint for the future.

Key words: Meteorites, Asteroids, 433 Eros, NEAR Mission, Spacecraft missions, Asteroid Chemistry, Asteroid Geology, Meteorite-asteroid links

Introduction

Nearly two centuries have passed since the studies of asteroids and meteorites first intertwined. E.F.F. Chladni first proposed an extraterrestrial origin for meteorites in 1794 (Chladni 1794; Marvin 1996), while Giuseppi Piazzi discovered the asteroid 1 Ceres on 1 January 1801. Almost immediately, a number of scientists, including Chladni, argued that asteroids were the remnants of an exploded planet and the source of meteorites falling to Earth (Burke 1986). It would take another decade for the extraterrestrial origin of meteorites to be widely accepted and nearly 50 years for the discovery of the first 10 asteroids. The idea that the vast majority of meteorites originated from asteroids that were themselves relics from the birth of the Solar System did not gain wide acceptance until the latter half of the 20th century.

At the end of the 20th century, our knowledge of both meteorites and asteroids had expanded tremendously. Laboratory studies of meteorites reveal that they originated from a compositionally diverse family of parent bodies that experienced a wide range of aqueous alteration and heating. These processes produced rocks ranging from primitive cosmic sediments (the chondrites) to a suite of irons, metal-silicate mixtures (pallasites) and basalts (eucrites) representing the cores, mantles and crusts of fully-melted worlds. Similarly, comparison of Earth-based telescopic spectra of asteroids and the reflectance spectra of meteorites suggested that the asteroids also sampled a full range of alteration, heating and melting. Two major questions remained unanswered. Which asteroids are the parent bodies to which meteorites? With rare exceptions, it has proven difficult or impossible to link specific asteroids to specific meteorites. In some cases, certain spectral classes of asteroids seem to match types of meteorites reasonably well, although a direct link between an individual asteroid and individual meteorite has proven elusive. In other cases, whole classes of meteorites seem to have no counterpart in the asteroids and *vice versa*. The second question is how did asteroids evolve during the 4.5 billion years that separates the formation of meteorites in original parent bodies and the modern asteroids that we can observe using Earth-based telescopes and spacecraft. How have 4.5 billion

years of meteorite bombardment and exposure to space changed the appearance of the asteroids?

In the last decade of the 20th century, a new era in asteroid exploration began with the advent of spacecraft observations. On 29 October 1991, the Galileo spacecraft made the first close approach to an asteroid, passing within 1600 km of 951 Gaspra and collecting images and spectra. On 28 August 1993, Galileo encountered the 58 km long asteroid 243 Ida and discovered a roughly equidimensional ~1.5 km diameter moon (Dactyl) orbiting within 90 km of Ida. These two flybys provided our first detailed look at asteroids, revealing asteroid geology for the first time. The flyby exploration of asteroids continued with the Near Earth Asteroid Rendezvous (NEAR) spacecraft encounter with 253 Mathilde on 27 June 1997 (Veverka et al. 1997) and the 28 July 1999 encounter of the Deep Space 1 spacecraft with asteroid 9969 Braille (Oberst et al. 2001). Although these flybys provided valuable data about asteroids, each was brief, lasting only a few hours and allowing for only quick examination. The culmination of these efforts occurred on 14 Feb 2000, when the NEAR spacecraft (by then renamed NEAR Shoemaker to honor the late pioneering geologist Eugene Shoemaker) entered orbit around the asteroid 433 Eros for a year of detailed observation of the geology, mineralogy and chemistry of the surface (Cheng et al. 1997, Veverka et al. 2000). This paper reviews the scientific results of that groundbreaking mission.

Spacecraft and mission profile

The Near Earth Asteroid Rendezvous mission was the first of NASA's Discovery missions, designed to probe the solar system "faster, better, cheaper". NEAR was developed, designed and built by the Johns Hopkins University Applied Physics Laboratory (APL) in 26 months. The entire mission cost $220.4 million, including $113.3 million for spacecraft development, $44.6 million for launch support and tracking, and $45.1 million for mission operations and data analysis. The 805 kg NEAR spacecraft was launched from Cape Canaveral Air Station, Florida, on 17 Feb 1996 on a mission that would last five years (Fig. 1). Summaries of mission strategies and spacecraft and instrument descriptions can be found in Russell (1997). On 27 June 1997, NEAR had a 25 minute encounter with asteroid 253 Mathilde, passing within 1212 km of the surface (Veverka et al. 1997). The encounter allowed the NEAR science team to collect images and spectral reflectance data, but was too brief to collect data on the chemical composition of the asteroid. Results of NEAR's encounter with Mathilde are summarized by Veverka et al. (1999). On 23 January 1998, NEAR made a swingby of Earth, with closest approach at 540 km over Iran. The Earth flyby provided a gravity assist to bend NEAR's orbital trajectory 11° out of the plane of the ecliptic, matching the orbit of its ultimate target – 433 Eros (Izenberg and Anderson 1998). During the flyby, NEAR collected images of the Middle East, Africa and Antarctica.

The NEAR mission was supposed to enter orbit around 433 Eros on 10 Jan 1999. On 20 Dec 1998, a scheduled 20 minute main engine burn was aborted and contact with the spacecraft was lost for ~27 hours and the planned orbital insertion was cancelled. On 23 Dec 1998, the NEAR spacecraft made a contingency flyby of Eros at a distance of 3800 km collecting images, spectra, and magnetic data (Veverka et al. 1999). A second main engine burn on 3 Jan 1999 placed NEAR in essentially the same orbit as Eros, with

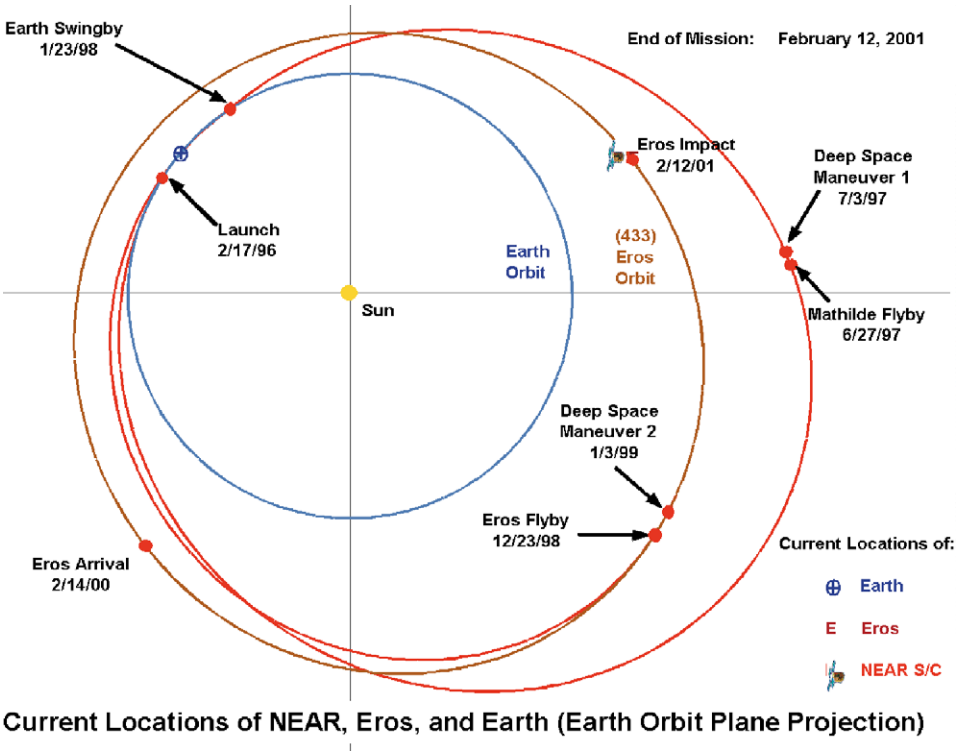

Fig. 1. Trajectory of NEAR Shoemaker from launch on 17 Feb 1996 to Eros touchdown on 12 Feb 2001. Locations of Earth, Eros and NEAR on 12 Feb 2001 are shown.

a new orbital insertion date of 14 Feb 2000 (St. Valentine's Day, which seems particularly appropriate given that Eros is named for the Greek god of love). NEAR entered orbit as planned on 14 Feb 2000 at a distance of 327 kilometers (Veverka et al. 2000). Over the next year, NEAR completed 230 orbits of Eros at distances ranging between 35 and 200 km from the center of mass of Eros. During this time, NEAR acquired more than 140,000 useful images of Eros (Bussey et al. 2002, Robinson et al. 2002a). The spacecraft initially orbited at an altitude of 200 km, providing regional coverage (typical angular resolution ~20 m/pixel) of the then-illuminated northern hemisphere. From February to July of 2000 the orbit radius was decreased in discrete steps down to 35 km, at which point the X-ray/gamma-ray spectrometer team controlled pointing for chemical mapping of the surface. The orbit was stepped back up to 200 km by November, thus allowing synoptic imaging of the then-illuminated southern hemisphere. At the outset of the orbital mission, the sub-solar point lay in the northern hemisphere, crossing into the southern hemisphere on 26 June 2000. While the higher altitude data provided regional coverage, the lower orbits (35–50 km) yielded high-resolution images (better than 5 m/pixel) showing the nature of the surface in great detail. In addition the spacecraft conducted a Low Altitude Flyover (LAF) in October 2000 when it passed within 6 km of the surface, collecting images at better than 1 m/pixel (Veverka et al. 2001a; Cheng et al. 2001). A further set of even closer Low Altitude Flyovers were conducted in late January 2001,

Fig. 2. The NEAR Shoemaker spacecraft. a – Artist's conception of the spacecraft in its post-launch configuration. Distance from tip to tip of the solar panels is ~5.2 m. b – The instruments which form the scientific payload of the NEAR Shoemaker spacecraft and their positions. Four of the instruments were fixed mounted on the aft deck, while the magnetometer was mounted above the high gain antennae.

with the spacecraft descending to within 3 km of the surface (image resolution better than 50 cm/pixel) (Veverka et al. 2001b). These maneuvers allowed the collection of approximately 776 images with sub-meter resolution. The near-infrared spectrometer failed on 13 May 2000, resulting in only limited coverage of the southern hemisphere. On 12 Feb 2001, NEAR executed a flawless descent to the surface after traveling nearly 3.7 billion kilometers during its journey. In the last phase of the descent, the spacecraft acquired 68 images with resolutions ranging from 60 cm down to 1 cm/pixel (Veverka et al. 2001b). Although mission planners expected the termination of the mission at this point, continued communication was possible through the low gain antennae from the surface of Eros. A two-week extended mission was granted to allow the first science ever conducted on the surface of a small body. This period was used to conduct gamma-ray spectroscopy and magnetic measurements of the surface. The NEAR mission terminated on 28 Feb 2001 – 5 years and 11 days after its launch.

NEAR Shoemaker was a solar-powered spacecraft (Santo et al. 1995) with a dry mass of 468 kg and carried an additional 337 kg of propellant at launch (Fig. 2a). After post-launch deployment of the solar panels, the spacecraft measured ~5.2 m from edge to edge of the solar panels. NEAR carried six scientific instruments (Fig. 2b). The magnetometer was mounted on the top of the high gain antennae, minimizing its exposure to magnetic fields from the spacecraft. The aft deck hosted the fixed-mounted multi-spectral imager, near-infrared spectrometer, X-ray spectrometer, gamma-ray spectrometer and laser rangefinder, all of which were co-aligned to a common bore sight. In addition, the radio science experiment team used the radio transponder to map the asteroid's gravity field and mass, and in conjunction with other instruments, determine the asteroid's density.

The instruments are described in detail in a special issue of *Space Science Reviews* (1997, Vol. 82, Nos. 1–2). Here we describe the major features very briefly. The multi-spectral imager and near-infrared spectrometer measured the spectra of sunlight reflected from the surface of 433 Eros to determine its silicate mineralogy by examining spectral absorption features at ~1 and ~2 microns produced by transition metal ions in olivine and pyroxene. The multi-spectral imager (Hawkins et al. 1997) provided high-resolution orbital images of Eros using seven narrow band filters from 0.45–1.05 μm at spatial resolutions down to better than a meter. The near-infrared spectrometer (Warren et al. 1997) measured 0.8–2.6 μm reflectance spectra with spatial resolutions as high as ~300 m from orbit. The X-ray and gamma-ray spectrometers were designed to determine the surface elemental composition of Eros (Goldsten et al. 1997). The X-ray spectrometer (XRS) detected photons in the 1–10 keV energy range, emitted from atoms in the top 100 microns of the asteroid's surface. The excitation source for the fluorescent emission was X-ray flux emitted from high temperature plasma in the Sun's corona. This instrument allowed for detection of characteristic X-rays from Si, Al, Mg, S, Ca and Fe. The gamma-ray spectrometer (GRS) detected 1–10 MeV photons arising from depths of tens of centimeters. Gamma rays are produced in planetary surfaces both by decay of naturally occurring radioactive elements and by cosmic-ray interactions with constituent nuclei. During the orbital mission, gamma-ray emissions from the surface were lower and detector background higher than expected and, thus, compositional interpretations are limited to Fe, Si, O, Mg and K abundances in the ~1 m^3 surrounding the gamma-ray spectrometer during the landed operations on the surface of Eros. The laser rangefinder (Cole et al. 1997) used a Cr-Nd-YAG laser to send a short burst of laser light to the surface of Eros and measured its return time. Internal in-flight calibration was provided by sending a

portion of each burst through a fiber optic cable of known length. A global shape model with a horizontal resolution of about 400 m was produced (Zuber et al. 2000). The fluxgate magnetometer (Lohr et al. 1997) was designed to measure the global magnetic field of Eros with an accuracy of ±5 nT.

The S-type asteroid 433 Eros was an ideal target for examining some of the fundamental questions about the geologic history of asteroids and their relationship to meteorites. Based on reflectance spectroscopy, S asteroids are believed to be composed of variable proportions of olivine, pyroxene and Fe,Ni metal. Gaffey et al. (1993a) have subdivided the S asteroids into S(I) to S(VII) with compositions ranging from olivine-rich to orthopyroxene-rich. Murchie and Pieters (1996) compiled 0.33–2.5 µm spectra of 433 Eros, the second largest of the near-Earth asteroids, grouping it as an S(IV) asteroid in the scheme of Gaffey et al. (1993a). Further, Murchie and Pieters (1996) noted rotational heterogeneity in the spectra of Eros, suggesting that one side was more olivine-rich and the other more pyroxene-rich. The work of Murchie and Pieters (1996), in the context of the Gaffey et al. (1993a) classification scheme, provided some extremely interesting possibilities for the geology and mineralogy of Eros. A heated debate has raged about the relationship between ordinary chondrites, the most common meteorite type among observed falls, and S asteroids, the most common type of asteroid in the inner belt (Gaffey et al., 1993b). Some authors (e.g., Wetherill and Chapman, 1988) suggest that S-class asteroids are the source of ordinary chondrites, despite spectral mismatches. Others (e.g., Bell et al., 1989) suggest that S-class asteroids originate from differentiated bodies, perhaps akin to the “primitive achondrites”, a wide range of meteorite types which have experienced varying degrees of partial melting and melt migration while retaining a mineralogical assemblage of olivine, pyroxene and Fe,Ni metal. Gaffey et al. (1993a) suggest possible meteorite types related to S(IV) asteroids, including ordinary chondrites, orthopyroxene-bearing ureilites, lodranites, winonaites and IAB irons.

Surface morphology and structure

Eros is an irregularly shaped body described by a best fit ellipse of 35 by 10.2 by 10.2 km (Veverka et al. 2000). The complete multispectral dataset has revealed a surprisingly complex surface including the existence of a global regolith (Veverka et al. 2001a, 2001b; Cheng et al. 2001; Robinson et al. 2001, 2002b) with an asymmetrically distributed population of boulders (Thomas et al. 2001), a heavily cratered surface at diameters above 200 m (Veverka et al. 2000; Chapman et al. 2002), and grooves and ridges thought to record broad scale tectonic deformation of the asteroid (Wilkison et al. 2002; Prockter et al. 2002; Thomas et al. 2002).

At the broadest scale the irregular shape of Eros is dominated by heavily degraded and rounded concave and convex sides (Fig. 3). The convex side is defined by 4 semi-flat facets while the concave side is composed of a single curved surface. On the convex side is a ~10 km depression (Himeros) that is superposed by the complex crater containing Shoemaker Regio. On the concave side of Eros is the relatively well-defined 5.3 km diameter bowl shaped crater Psyche (Veverka et al. 2000; Thomas 2001). At the next level of detail (1 km to 100 m scale), Eros is marked by a series of groove and ridge patterns that show many orientations superposed on a heavily cratered surface (most areas saturated at >200 m diameter craters (Veverka et al. 2000, 2001a; Prockter et al.

Fig. 3. Four synoptic views of Eros, the two mosaics on the left were taken early in the mission when the Sun was in the northern hemisphere, and the two on the right late in the mission when the Sun was illuminating the southern hemisphere (Upper Left: 127504836-127521356; Lower Left: 126036009-126036283; Upper Right: 149409043-149409291; Lower Left: 149639534-149639530).

2002; Chapman et al. 2002; Wilkison et al. 2002, Robinson et al. 2002b)). Finally, at the <100 meter scale the asteroid morphology is dominated by boulders, slides, streamers, ponds, and other features indicative of regolith accumulation and transport. Surprisingly the surface is relatively depleted in small craters (<100 m diameter) (Veverka et al. 2001a; Chapman et al. 2002). At all scales the majority of surface features are rounded or infilled indicating a relatively mature state.

Stratigraphic Relations of Major Features

The largest feature identifiable on Eros is the depression Himeros (probable impact crater, 10 km across, 1.5 km deep). The major process that forms topographic features on asteroids is impact cratering, and such an event most likely formed Himeros (Fig. 4, 5). Its elongate shape may be due to wall failure as the crater exceeded the radius of the asteroid in the north-south direction during the impact event. In images acquired with extreme lighting conditions, and in the shape model, a raised rim is visible around most of the feature, a morphology consistent with an impact origin (Robinson et al. 2002b). The interior of Himeros is less cratered than much of Eros and contains exposed fault scarps, slump materials, and boulders: clear evidence that the interior is resurfaced and is thus younger than the actual depression.

The depression containing Shoemaker Regio (Fig. 4, 5) is 7 km across and several hundred meters deep and superposes the southwest rim of Himeros (showing it to be younger). The interior has few craters and is covered with boulders, slumps, and what appears to be a relatively thick and unconsolidated layer of regolith which composes

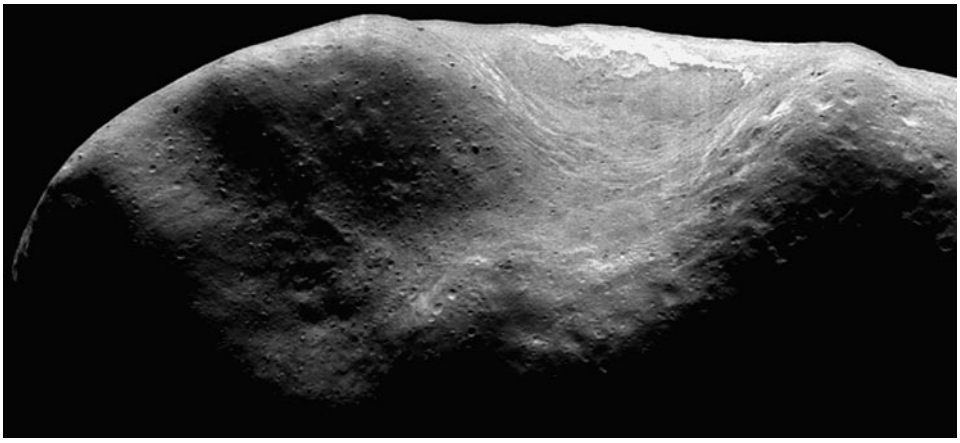

Fig. 4. Equatorial latitudes centered on Shoemaker Regio (left – ~7 km diameter) and Himeros (right), lighting is from the north. Note the superposition of Shoemaker Regio on Himeros showing it to be younger (127733021-127733455).

Fig. 5. Left: View from southwest rim across to northeast rim of Himeros (141204041-141204537) Right: Oblique view of northwest portion of Shoemaker crater, large boulder in upper center is ~120 m in diameter, downslope is from upper left to lower right 136402682–136403178).

Shoemaker Regio, material most likely formed as a result of the impact event that created Shoemaker crater (for simplicity the crater that contains the Shoemaker Regio deposit will be referred to as Shoemaker crater in this paper, though the name has not been approved by the IAU). The interior of Shoemaker crater is segmented into four depressions indicating pre-existing structure, multiple overlapping impacts, or possibly impact of a fractured highly irregularly shaped (?) bolide. Similar to Himeros, Shoemaker crater

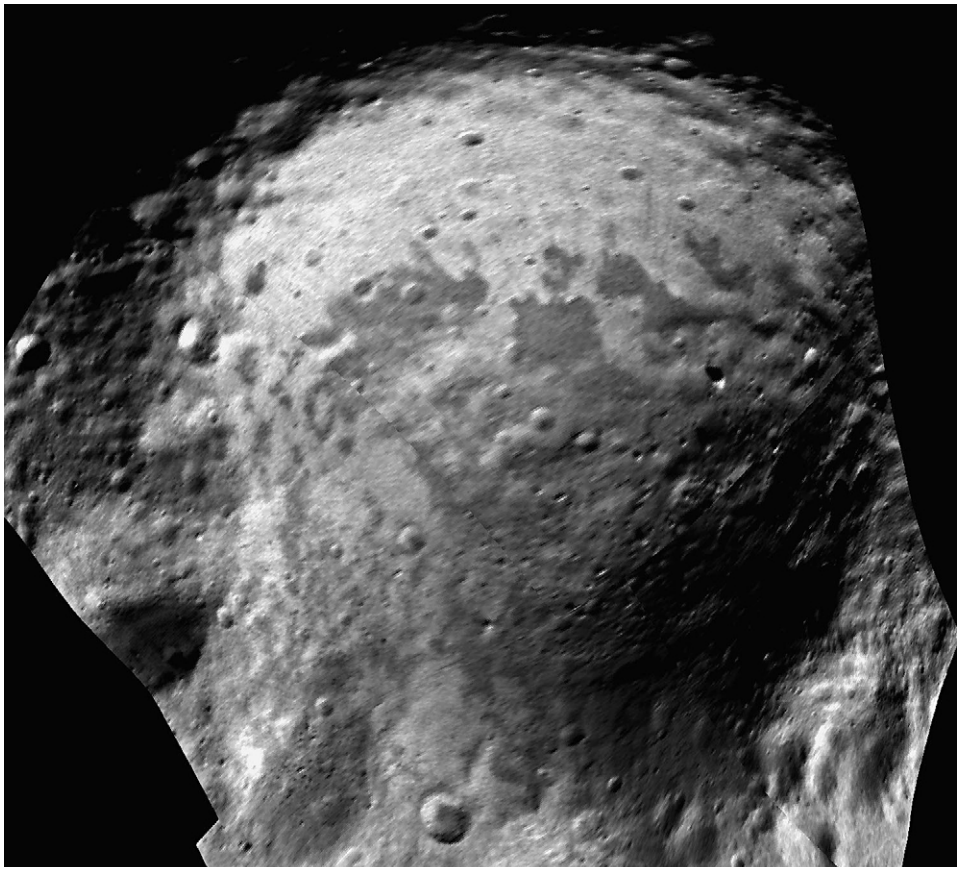

Fig. 6. Mosaic centered on Psyche crater (5.3 km diameter, north to the top; 143963632-143963818).

is large enough that its walls probably failed during crater growth resulting in its low depth-to-diameter ratio and smoothed rim.

The largest clearly identifiable impact crater on Eros is Psyche (5.3 km diameter, ~1 km deep, Fig. 3, 6). Psyche appears relatively unmodified or degraded and has depth/diameter ratio approaching the lunar value of 0.2 for simple bowl shaped craters (Pike 1977), implying a young age. Relative age relations between Himeros, Shoemaker crater, and Psyche crater are not necessarily clear-cut. Psyche exhibits the freshest morphology, but its southern rim is cut by at least four 1 km craters: the highest population of superposed 1 km (or larger) craters of the three features, thus arguing that it is an ancient feature despite its youthful appearance. Since the area of Psyche is small, the crater counts may be statistically unreliable yielding faulty relative age relations. Modeling of ejecta patterns from the largest craters on Eros indicate that the boulder pattern found on the east wall of Psyche is consistent with emplacement as secondaries formed by impact ejecta from Shoemaker crater (Fig. 6) (Thomas et al. 2001). Thus, it is likely that Shoemaker crater is the youngest of the three features, and Himeros is the oldest.

Structure

Structural features are abundant on Eros and include chains of craters, sinuous and linear depressions, ridges and scarps, and rectilinear craters (Fig. 7) (Veverka et al. 2000; Prockter et al. 2002; Thomas et al. 2002). The large variation in directions, patterns, and relative ages of the lineations indicate that they were formed in many different events throughout the history of the asteroid (Veverka et al. 2000; Prockter et al. 2002; Thomas et al. 2002). A subset of the grooves have pitted segments, similar to grooves found on the martian moon Phobos interpreted to indicate draining of loose material into interior void. Rahe Dorsum (Fig. 8) is a prominent ridge system that spans the northern hemisphere and geometrically defines a planar slice through the asteroid (Veverka et al. 2000; Thomas et al. 2002). This ridge cross-cuts Himeros and possibly Psyche crater, indicating that it was created after Eros reached its current shape. Small segments of Rahe Dorsum form cliffs with slopes above the angle of repose (Cheng et al. 2002) indicating a high degree of interior cohesive strength. This scarp is continuous across more than a third of an Eros circumference and its morphology is consistent with a compressive fault plane through consolidated or cohesive material. A set of parallel twisting ridges (Callisto Fossae) on the opposite side of Eros may represent the continuation of this same fault, or plane of weakness: here the morphology is more consistent with an extensional environment, possibly indicating a hemispheric distortion of the asteroid about this plane (Thomas et al. 2002). Morphological features such as regions of high slopes, continuous grooves, steep continuous ridges, and fault planes all suggest that the asteroid possesses global mechanical strength and is not strictly a gravitationally bound granular object (Thomas et al. 2002, Wilkison et al. 2002; Zuber et al. 2000).

Radio science measurements of the mass (Yeomans et al. 2000) when combined with an image based volume of Eros allow the calculation of bulk density of 2.67 ± 0.03 g/cm^3

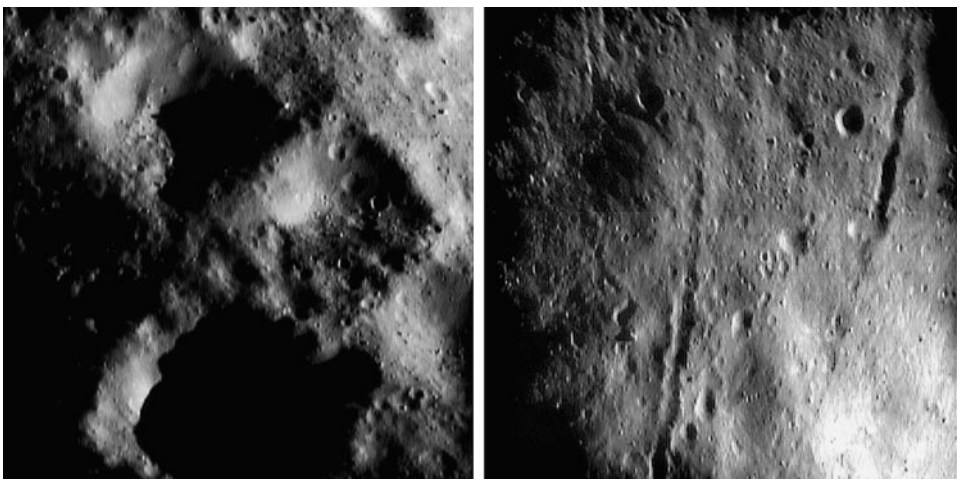

Fig. 7. Two panel Fig. showing rectilinear crater indicating pre-existing joint control (square crater center right ~900 m diameter, 132151511-132151569) and grooves (~1.4 km frame width 135343994), both features require a cohesive substrate (Wilkison et al, 2002).

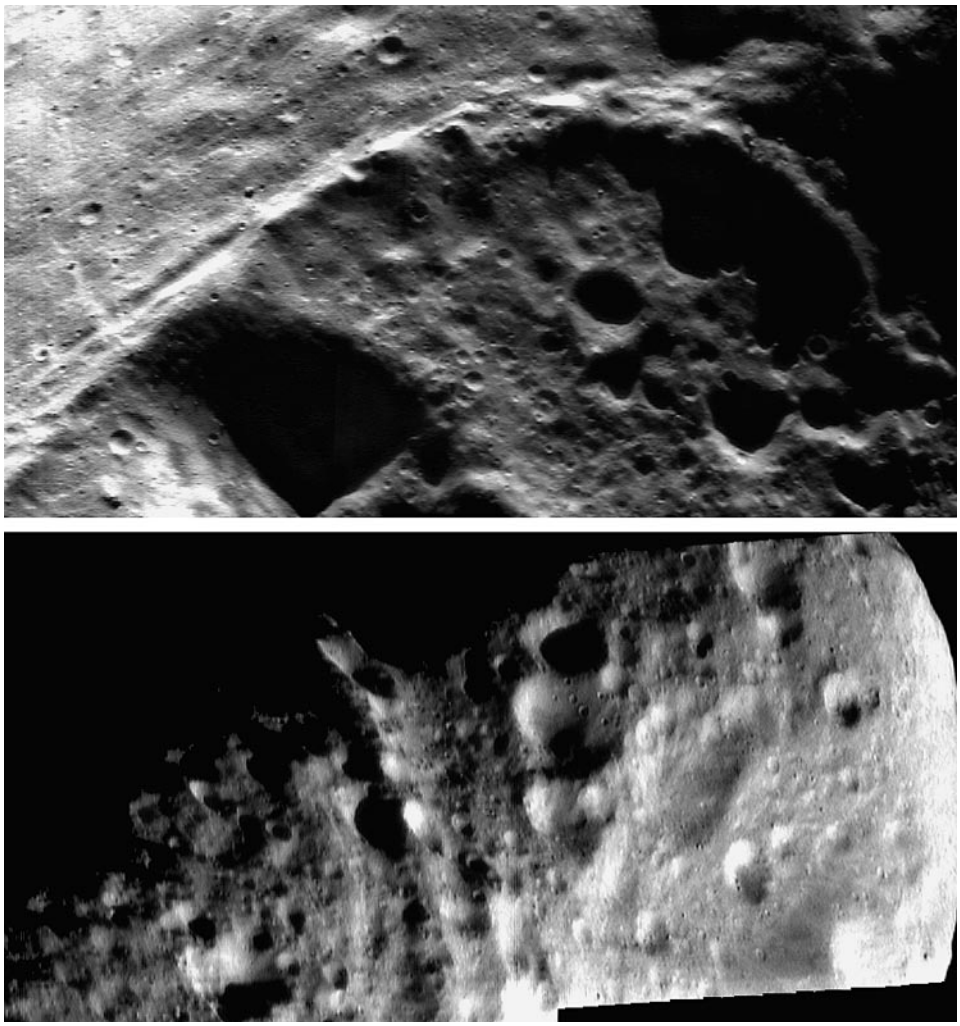

Fig. 8. Top: Large scarp that spans 1/3 of an Eros short diameter (Rahe Dorsum) interpreted to be a large scale fault (scene width ~4 km, 131893649, 131893737, 131893825). Bottom: Trough and ridge feature possibly indicating extensional faulting, known as Callisto Fossae (distance between ridges ~900 m, 131177449, 131177643).

(Veverka et al. 2000). Most compositional and mineralogic estimates for Eros (discussed below) are consistent with a bulk ordinary chondrite composition. Laboratory measurements of ordinary chondrite densities (3.4 g/cm^3) indicate that Eros has an internal macroporosity (large scale fracturing) of ~20% (Wilkison et al. 2002). This porosity value is consistent with the morphologic interpretation that Eros has experienced large scale internal fracturing, but remains relatively intact (Veverka et al. 2000; Wilkison et al. 2002).

Regolith

In nearly every image of Eros taken from 50 km or lower orbits (better than 5 m/pixel) evidence for a layer of loose fragmental debris, or regolith, is visible. Features include, smooth talus deposits, downslope streamers, partially buried boulders and craters, and a class of deposits referred to as "ponds" (Veverka et al. 2001; Robinson et al. 2001; Thomas et al. 2001; Cheng et al. 2001). Slopes on Eros average about 10° (Zuber et al. 2000). Those slopes above 25° generally show higher albedos, reduced boulder populations, and morphologic evidence for downslope motion of loose materials (Fig. 9) (Veverka et al. 2000; Clark et al. 2001; Murchie et al. 2002). A comparison of the depth of relatively fresh craters to smooth craters indicates an infilling of a few m to 150 m deep, with a median at 20–30 m. Large scale deposits of debris (both boulders and fine

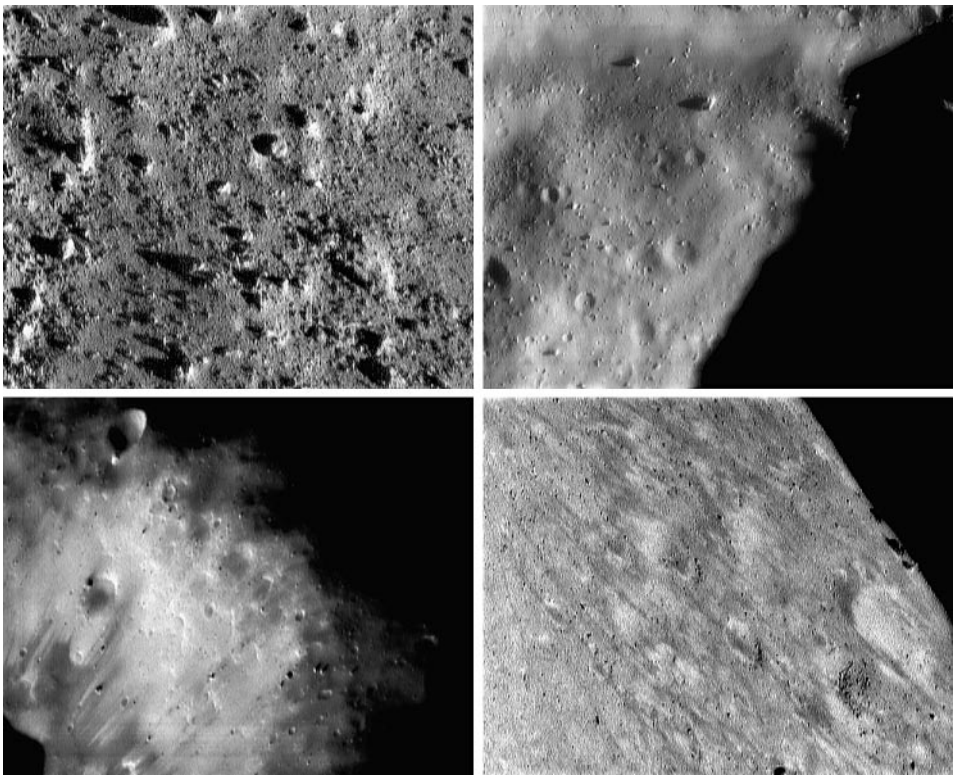

Fig. 9. Evidence of a loose fragmental layer of debris (regolith) on the surface of Eros comes in many forms. Upper Left: Unconsolidated poorly sorted debris in the floor of Shoemaker crater (156082066, frame width 700 m). Lower Left: downslope movement of relatively fine, high albedo particles inside of Selene crater, downslope is from upper right to lower left (133161713, frame width 1600 m). Upper Right: Smooth deposits along top edge of frame are talus shed from steep scarp inside Himeros just outside of frame, note also the degraded nature of impact craters (13475422, frame width 1400 m). Lower Right: Streamers showing downslope movement of materials on east wall of Himeros. Note how streamers are insensitive to local topographic barriers such as crater walls, downslope is from lower right to upper left (140996328, frame width 7000 m).

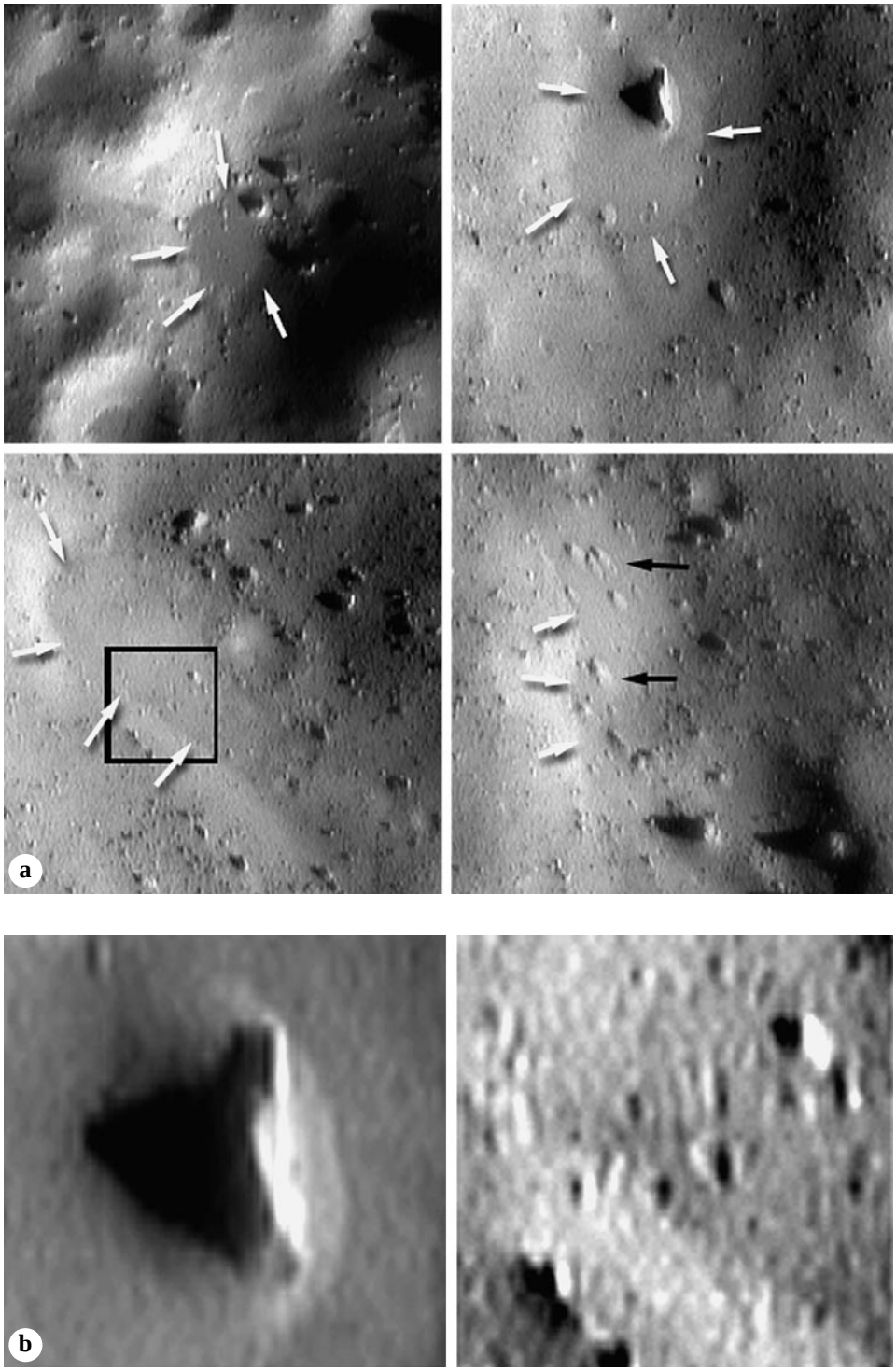
a
b

grained material) in for example, Shoemaker Regio, equal at least 80 m of regolith (Barnouin-Jha 2000; Thomas et al. 2001). In addition, if features seen within Eros's grooves are interpreted as drainage pits, then the regolith could be as much 50–100 m thick (locally) from the models of Veverka et al. (2000) and Thomas et al. (2001). A pervasive covering of loose material would be highly mobile during impact triggered seismic events, and could erase small craters and partially to wholly bury boulders, resulting in a morphology consistent with that seen on Eros (partially buried relief features, infilled and degraded craters, paucity of small craters). Such seismic redistribution of regolith materials has been proposed to explain subdued topography and smooth floored craters on the Moon (Schultz and Gault 1975). Impact craters on Eros show little obvious evidence of layers in their walls or the morphologic effects of mechanical discontinuities at depth such as some lunar mare craters do (Oberbeck and Quaide 1968), or some craters on Phobos (Thomas et al. 2000). Such discontinuities on other bodies and in laboratory simulations are attributed to the interface between a regolith and coherent substrate (Quaide and Oberbeck 1968; Oberbeck and Quaide 1967, 1968). This general lack of discontinuities in small crater walls on Eros suggests highly fractured materials with properties changing gradually with depth to many tens of meters or in some areas well over 100 meters (Robinson et al. 2002b).

Eros is littered with tens of thousands of boulders larger than 10 m in diameter (Thomas et al. 2001). Their morphology ranges from angular to fractured to disaggregated (Fig. 9). Most were probably emplaced as low velocity ejecta blocks from crater forming events on the asteroid. Their current morphologic state is most likely related to three key factors (in order of importance): original internal strength of the material composing the block, impact velocity, and exposure age on the surface. The number of boulders per unit area is high relative to averages for the Moon or Phobos (Veverka et al. 2001a ; Chapman et al. 2002). However it is well known that boulder density varies (factor of >100×) on the Moon (Lee et al. 1986; Cintala and McBride 1995; Thomas et al. 2001). Since Eros has a surface area of only 1,125 km^2 a single cratering event such as Psyche, Himeros, or Shoemaker Regio could be responsible for much of the asteroid boulder population. Consistent with this idea it is known that lunar boulder densities in and around specific craters reach values greater than that found in the area of highest boulder density on Eros, Shoemaker Regio (Lee et al. 1986; Cintala and McBride 1995; Thomas et al. 2001). Modeling the ejecta patterns of the largest craters on Eros indicates that the majority of boulders currently seen on Eros were emplaced during formation of crater Shoemaker (Thomas et al. 2001). This result not only indicates that the boulder population is not necessarily unusual (relative to the Moon) but also clarifies the stratigraphic relations between Shoemaker crater and Psyche crater (Psyche is older, see above discussion).

◀ **Fig. 10a.** Examples of "ponded" deposits, white arrows show embaying margins, and black arrows indicate aprons of material apparently draped over pre-existing topography (upper left 147932871, frame width is 1600 m, upper right 147953478, total width 290 m, lower left 147953378 total width 300 m, lower right 147953203, total width 340 m) **10b**. Left: Enlargement of block with sediment apron seen in upper right panel of Fig. 10a. Right: Enlargement of pond and crater floor it embays, location indicated with black box in lower left of 10a. Note the small negative relief features with raised rims in the pond showing that it currently has some degree of internal cohesion.

A surprise of the mission was the discovery of a family of smooth deposits that are seen to infill depressions (Fig. 10) (Veverka et al. 2001a, b; Robinson et al. 2001). The margins of these deposits typically sharply embay their surroundings and their surfaces are generally perpendicular to the local gravity gradient. The observation that these deposits represent an equipotential surface led to the interpretation that they were emplaced with no shear strength (fluid-like flow) thus giving rise to the term "ponded deposits", or more simply "ponds" (Veverka et al. 2001). Since all evidence points to the conclusion that Eros is a compositionally primitive and homogeneous body (Bell et al. 2002; Trombka et al. 2001; Evans et al. 2001; Acuña et al. 2002; Murchie et al. 2002) it is unlikely that the ponds represent a separate rock type. Rather, the ponds were proposed to represent fine sediments sorted from a regolith with a range of grain sizes (Robinson et al. 2001). Not only do the ponds have a unique morphology, they also exhibit distinct color properties; they are relatively blue (550/760 nanometer ratio) and have an enhanced mafic band (950/760 nanometer ratio). Pond color properties are consistent with a concentration of fresh crystalline material, relatively unaffected by space weathering. Of the 255 ponds with diameters greater than 30 m, 91% were found to occur with 30° of the equator. Areas that contain the highest density of ponds also correspond to places on the asteroid that undergo extended periods of dawn and dusk (similar to lighting conditions at the polar regions of the Earth). Eros's vacuum environment and the extended terminator crossings near the equator are ideal environments for electrostatic levitation of the finest regolith particles (Lee 1996). Robinson et al. (2001) proposed that ponds might be formed by preferential movement of extremely fine material from the regolith into depressions via electrostatic levitation. The finest fraction might be relatively enriched in unaltered mineral grains. The coarser material that is left behind might be enriched in metal-rich clasts and space-weathered glasses known as agglutinates, which by definition are larger size fractions as they are clumps of fines held together by impact induced quenched melt. This type of segregation and transport explains the unusually smooth nature of the ponds along with the observed color contrasts. Other processes such as seismic shaking may also play an important role in redistributing regolith components and more work is needed to understand the complicated nature of sedimentary processes on asteroids.

Descent to the Surface

The spacecraft's multi-spectral imager acquired 68 images with resolutions ranging from 60 cm down to 1 cm/pixel during its descent to the surface (Veverka et al. 2001b). These images further confirmed the interpretation that the entire surface is covered by a regolith and shed some further light on centimeter scale processes. The ground track of the final images crossed over a rather unexceptional, heavily cratered portion of the asteroid (Fig. 11). These data showed that the general observation that Eros is deficient in small craters and has an abundance of boulders holds at the sub meter scale (Veverka et al. 2001b). In each descent image evidence can be found of loose fragmental debris in the form of infilled craters, partially buried boulders and cobbles, and ponded deposits. NEAR Shoemaker landed inside an ~100 m diameter crater, most likely on the surface of a pond (Fig. 12). In the final image it is apparent that ponds (at least this one is!) are smooth at the sub cm scale, consistent with previous interpretations that ponded deposits are composed of fine-grained material (Veverka et al. 2001a, b; Robinson et al. 2001). An

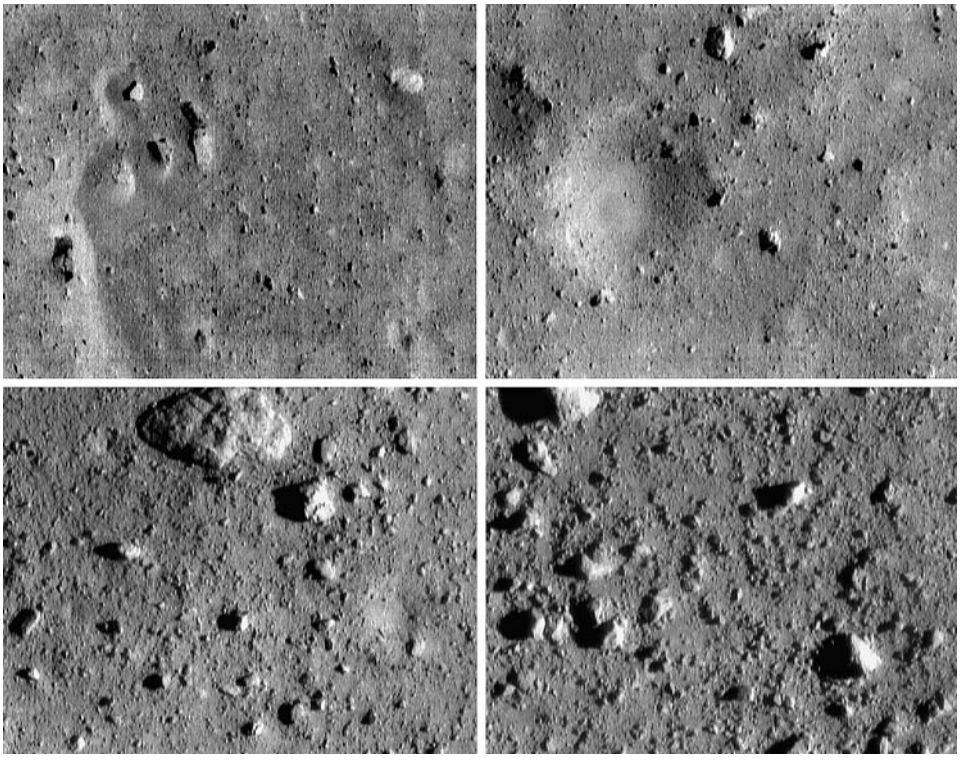

Fig. 11. Series of four images from descent sequence showing close up view of surface properties at unprecedented spatial resolutions. Note the infilling of craters, ponded materials, lack of sorting, and generally angular nature of surface blocks (Upper left 157415638 35 cm/pixel – frame 168 m width, Upper right 157416203 23 cm/pixel – frame 110 m width, Lower left 157416658 10 cm/pixel – frame 48 m width, Lower right 157416983 5.6 cm/pixel – frame 27 m width).

additional important outcome of the descent to the surface is the knowledge that asteroid surfaces can be a benign environment for future sample return spacecraft, and that a variety of material sizes (sub cm to meter) is available for sampling.

Mineralogy

The mineralogy of 433 Eros was determined by reflectance spectroscopy using the near-infrared spectrometer and multi-spectral imager. This technique, which is widely applied to Earth-based observations of asteroids, utilizes the distinctive absorption features present in the spectra of Fe^{2+}-bearing minerals (e.g., Burns 1993). In meteorites and asteroids, these spectral absorption features are primarily due to olivine and pyroxene and reflect their relative abundances and compositions. Olivine has a single asymmetric absorption feature centered at ~1 micron and made up of three separate absorption bands. In contrast, pyroxenes tend to have two bands centered at ~0.9–1.0 and ~1.9–2.0 microns. The positions of the three olivine bands move to longer wavelengths with

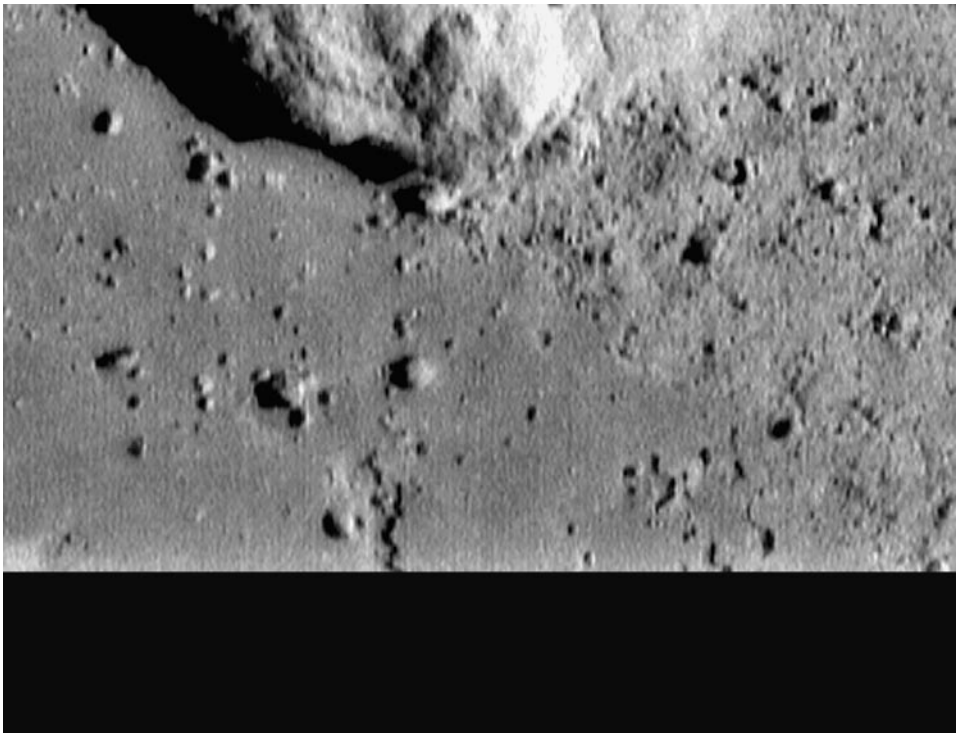

Fig. 12. Final image of the surface acquired by NEAR Shoemaker from a range of only ~129 m, the black area at the bottom represents portion of image lost when the spacecraft touched down on the surface and the antenna pointed away from Earth. Two sinuous "collapse pits" are just being revealed at the bottom of the frame possibly indicating subsurface drainage of fine loose material into a void (Veverka et al, 2001b). The spacecraft apparently landed on a pond seen coming into view in the lower left. From this image it is clear that ponded deposits are smooth down to the cm scale (157417198, 1.2 cm/pixel, frame width ~6m). An important finding of these final images (see also Fig. 11) is that there are a wide variety of grain sizes (sub cm to m) readily available for future sample return missions, obviating the need for complicated and costly drilling apparatus.

increasing iron concentration (Burns 1970), while the two pyroxene bands move to longer wavelengths with increasing iron and/or calcium concentrations (Adams 1974). The end result of these multiple absorption features and their dependence on mineral composition is that the band area ratio (Band II/Band I; 2 micron/1 micron) is a function of the olivine:orthopyroxene ratio while the band center positions reflect the composition of the olivine and pyroxene (Cloutis et al. 1986).

Understanding the mineralogical composition of Eros in the context of meteorites has been a major goal of the multi-spectral imager/near-infrared spectrometer science team for NEAR (McFadden et al. 2001; Bell et al. 2002). Eros's average reflectance spectrum has absorption features centered at 0.95 and 2.0 μm (Fig. 13) (McFadden et al. 2001), indicative of the existence of both olivine and pyroxene. The computed band area ratio (Fig. 14) (McFadden et al. 2001; Bell et al. 2002) for Eros indicates an olivine:pyroxene ratio of ~60:40, assuming a two-component mixture of these minerals. The Band I center

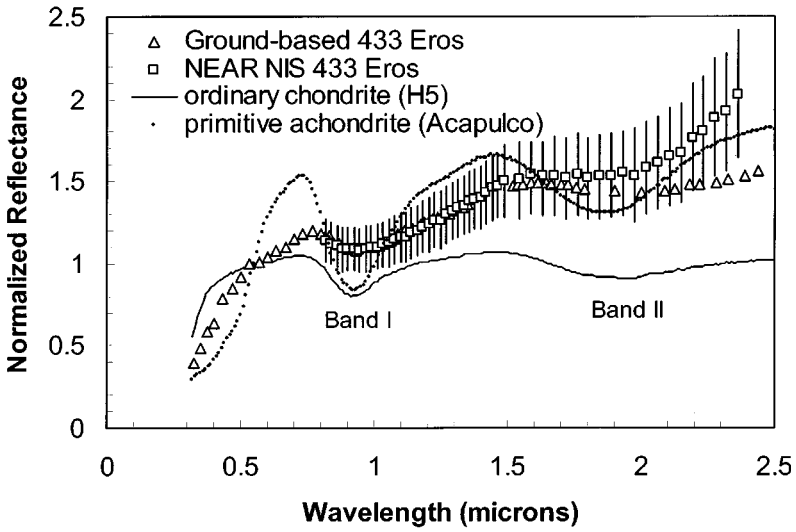

Fig. 13. Reflectance versus wavelength for 433 Eros. Triangles are ground-based spectra of Eros (Murchie and Pieters, 1996). Squares are the average NEAR-Shoemaker NIS spectra of Eros, normalized to the ground-based spectrum at ~0.8 microns. The line is the spectrum of an H5 ordinary chondrite and the dotted line is the spectrum of the primitive achondrite Acapulco. All spectra are normalized are normalized to unity at 0.55 microns.

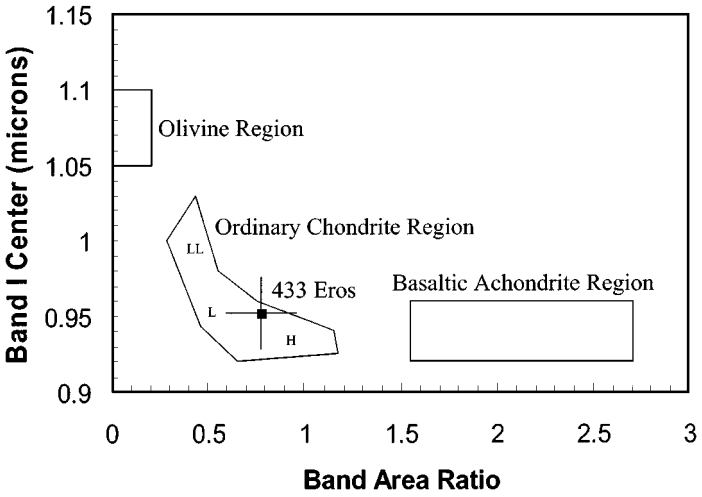

Fig. 14. Plot of band area ratio versus Band I center for 433 Eros and different types of meteorites, after Gaffey et al. (1993a). Eros can be seen to plot in the ordinary chondrite region.

position, band area ratio and derived olivine:pyroxene ratio of Eros are all consistent with those found in ordinary chondrites. McFadden et al. (2001) note that the olivine:pyroxene ratio is within the range for normative mineralogies of H chondrites determined by McSween et al. (1991). Primitive achondrites – meteorites which have experienced

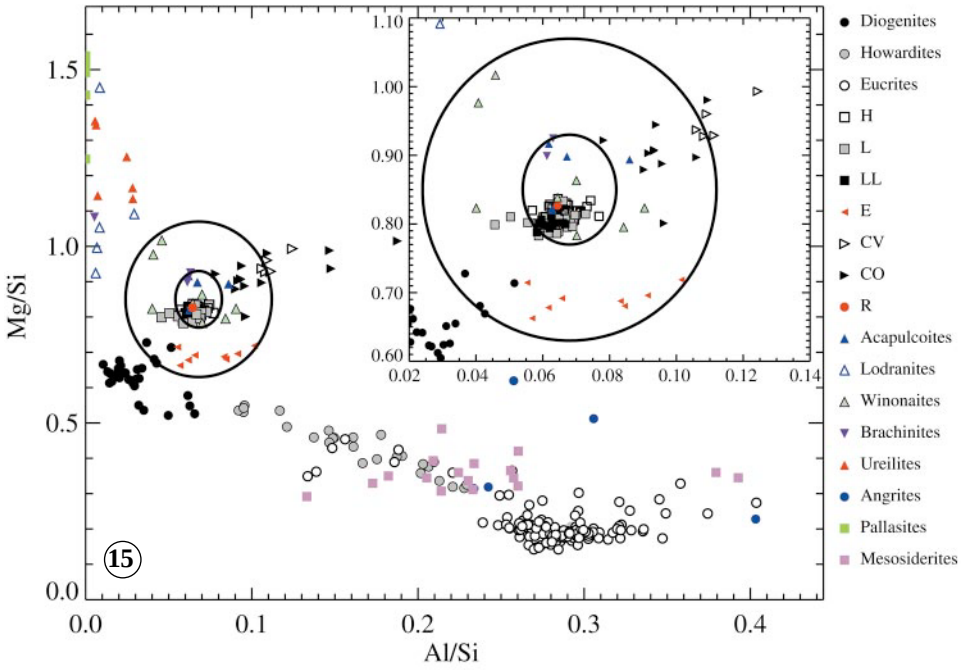
Mg/Si
Al/Si
15
Diogenites
Howardites
Eucrites
H
L
LL
E
CV
CO
R
Acapulcoites
Lodranites
Winonaites
Brachinites
Ureilites
Angrites
Pallasites
Mesosiderites

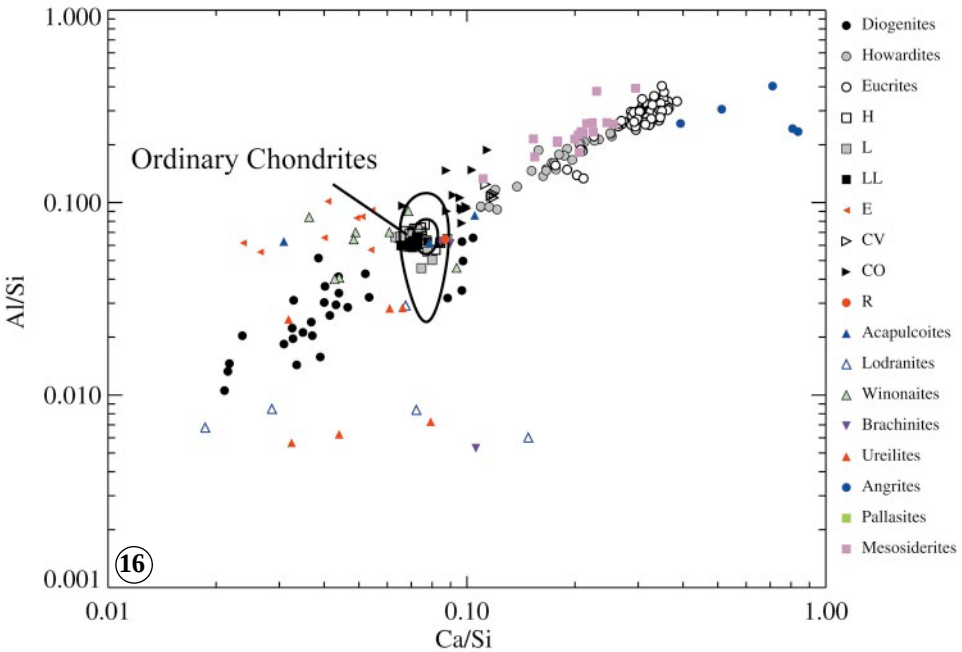
Ordinary Chondrites
Al/Si
Ca/Si
16
Diogenites
Howardites
Eucrites
H
L
LL
E
CV
CO
R
Acapulcoites
Lodranites
Winonaites
Brachinites
Ureilites
Angrites
Pallasites
Mesosiderites

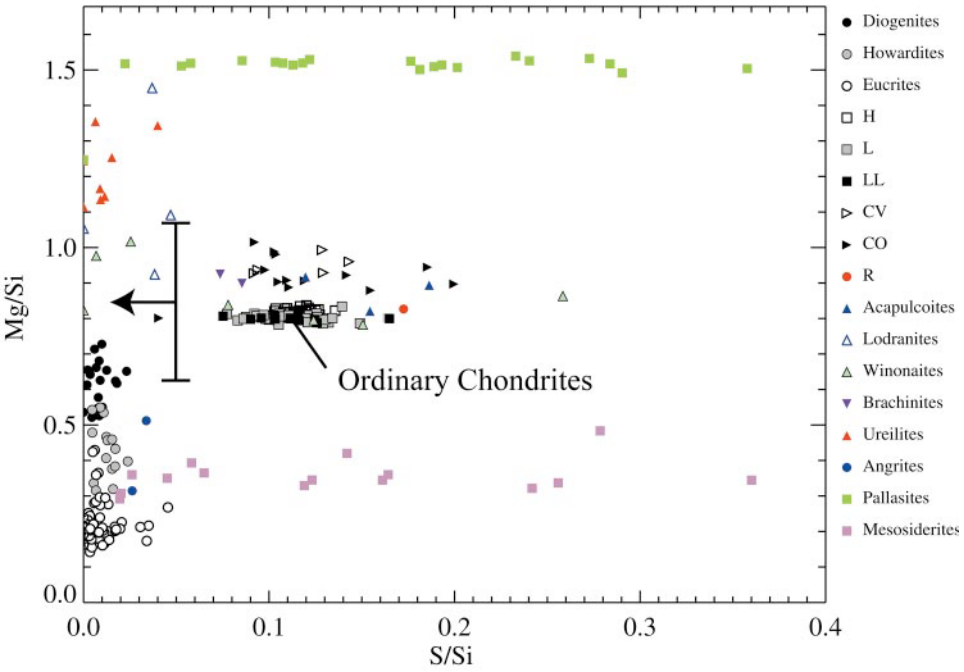

Fig. 17. Mg/Si and S/Si weight ratios of Eros with a variety of meteorite types. The S/Si ratio is a factor of 2 lower than observed in unweathered ordinary chondrites, probably reflecting surface depletion of sulfur, due to processing by impacts and/or radiation.

◀ **Fig. 15.** Average Mg/Si and Al/Si weight ratios for Eros plotted with a variety of meteorite types. The error ellipse is the 2σ variability in the data and is the allowed range of elemental heterogeneity between the sampled regions of Eros. The smaller ellipse represents 2× the standard error of the mean and represents the uncertainty in our knowledge of the average composition. The inset expands the chondritic region of the plot. The average Mg/Si and Al/Si abundances are similar to a wide range of chondrites (e.g, H, L, LL, CO, R) and primitive achondrites (e.g, acapulcoites, winonaites, brachinites), but differ from meteorites formed by extensive melting and differentiation (e.g, eucrites, lodranites), providing strong evidence against global melting and differentiation of 433 Eros.
[Fig. 15, 16 and 17: Reproduced from Nittler et al. (2001) X-ray fluorescence measurements of the surface elemental composition of asteroid 433 Eros. Meteoritics and Planetary Science 36, 1673–1695.]

Fig. 16. Average Al/Si and Ca/Si weight ratios for Eros (ellipses) with a variety of meteorite types. See Fig. 15 for explanation of error ellipses. The consistency of these ratios both with each other and with primitive, chondritic compositions, despite being subject to systematic errors which differ between the two, suggests that the total uncertainty is not significantly larger than reported by Nittler et al. (2001).

limited partial melting but retained their chondritic bulk compositions (Mittlefehldt et al. 1998) - tend to be either too olivine- or pyroxene-rich compared to Eros.

Olivine composition is difficult to determine given the presence of both an olivine and pyroxene absorption feature at ~1 μm. In contrast, the band II position (2.0 μm) for Eros can be used to constrain the pyroxene composition. Simultaneous solution of the relations between band II position and Ca and Fe concentration yields a single pyroxene of composition $Fs_{62}Wo_{15–18}$ (McFadden et al. 2001). This FeO-rich pyroxene composition is inconsistent with the derived olivine:pyroxene ratio of ~60:40 and would only be found in FeO-rich, pyroxene-dominated basaltic meteorites formed by extensive igneous differentiation. The band II position appears best matched by the presence of two pyroxenes (a low-calcium orthopyroxene and a high-calcium augite) (McFadden et al. 2001), similar to those found in ordinary chondrites. Although the band II position cannot uniquely define either the ratio of orthopyroxene:augite or the composition of the orthopyroxene, the best match among the ordinary chondrites is the LL chondrites (McFadden et al. 2001). Interestingly, this seems to be in some conflict with the derived olivine:pyroxene ratio, a subject we discuss in greater detail later in this paper.

A remarkable feature of Eros is that it is extremely uniform in its inferred mineralogy (Bell et al. 2002) and, like most asteroids, its spectrum is significantly redder (steeper) than spectra of analog meteorites measured in the laboratory. These authors found no regions of Eros that differed from the average olivine:pyroxene ratio outside the 1σ instrumental uncertainty. Remarkably, there are significant albedo differences across the surface and that high-albedo units are associated with specific steeply sloping (slopes above 25º) features (Murchie et al. 2002). While infrared color (defined as the ratio of reflectances at 0.950 μm and 0.760 μm) differ by only ~10%, the albedo (reflectance at 0.760 μm; corrected for viewing and illumination angles) varied by more than a factor of 2. Eros exhibits an order of magnitude less color variation with increasing reflectance than the Moon. Compared to other S-asteroids (Ida and Gaspra) observed by spacecraft, the range of reflectance variation on Eros is a factor of 2 larger, but the range of color variation is two to four times smaller. Murchie et al. (2002) found that as the surface slope increases, the surface becomes increasingly dominated by higher reflectance materials with lower 0.950 μm/ 0.760 μm color ratios. This appears to indicate the downslope movement of " relatively dark" component of the regolith, leaving behind "fresher," "less-altered" material. Using NIS data for the crater Psyche, Clark et al. (2001) also found that material on the steep slopes is brighter than the background material in and around the crater. However, none of the bright material has spectra that matched those of meteorites. Thus, even the "fresh" material appears redder than analog meteorites. This type of reddening is believed to be due to alteration of the surface layer of the asteroid in response to exposure to the space environment (e.g., micrometeorite impacts, solar wind sputtering) and these processes are collectively termed space weathering (e.g., Pieters et al. 2000; Sasaki et al. 2001; Hapke 2001). It is thought that these processes alter the spectra via production of glassy material (agglutinates) and vapor-deposited coatings of nanophase iron.

Magnetism

The NEAR spacecraft carried a magnetometer in hope of encountering a global scale magnetic field from 433 Eros. Results from the Galileo encounter with the S-type

asteroid Gaspra suggested a magnetic field based on perturbations in the interplanetary magnetic field (Kivelson et al. 1993) and Richter et al. (2001) recently argued for a high level of intrinsic magnetization of asteroid Braille based on data from the Deep Space 1 flyby. The NEAR magnetometer obtained extensive magnetic field observations at distances ranging from more than 100,000 km from Eros to those conducted on the surface after landing (Acuña et al. 2002). Surprisingly, Eros exhibits essentially no global scale magnetization (upper limits of ~1 nT for orbital observations, ~5 nT for surface observations (surface observations were subject to a greater uncertainty due to subsystem reconfigurations in preparation for landing and undetermined effects after landing)). Certainly the near complete absence of a global magnetic field points to a primitive, chondritic body that has not experienced significant heating or melting. However, the upper limit for global scale magnetization for Eros is well below that for laboratory samples of H, L and LL ordinary chondrites. The most likely explanation is that although the individual components (e.g., chondrules, metal grains) in chondritic meteorites can exhibit higher magnetization states (Morden and Collinson 1992), their random distribution within these rocks produces a much smaller global scale magnetization. In addition, the effects of brecciation and resulting randomization on asteroidal-sized bodies remain poorly constrained.

Chemical composition

The NEAR mission provided our first opportunity for remotely-sensed bulk chemical compositional studies of an asteroid using the X-ray (XRS) and gamma-ray (GRS) spectrometers. X-ray measurements were conducted throughout the orbital phase of the mission. Typical solar conditions ("quiescent") produced excitation of Mg, Si and Al from the surface of Eros. However, the solar X-ray flux varies with time and is greatly enhanced during solar flares, yielding much higher fluorescent flux from asteroid surfaces, consequently higher signal-to-noise ratios for NEAR XRS spectra and excitation of S, Ca, and Fe in addition to Mg, Si, and Al. Thus, periods of solar flares provided particularly valuable opportunities to understand the chemical composition of the surface of Eros. For a number of reasons (Trombka et al. 2001), the signal-to-noise ratio for the NEAR GRS was far less favorable than expected, with the result that no compositional data has yet been obtained from GRS spectra obtained during the year of orbital measurements. However, after the controlled descent to the surface on 12 Feb 2001, the spacecraft was in an ideal orientation for obtaining surface gamma-ray measurements and some seven days of high signal-to-noise GRS data were obtained from the surface. Complicating the comparison of the XRS and GRS data is the grossly different spatial scales of the measurements: the XRS data represent an average of several km-sized regions from across the asteroid; the GRS data represent a specific spot less than one meter across.

Preliminary compositional data for Eros were reported by Trombka et al. (2000) from XRS data acquired during two solar flares and a longer integration under more typical ("quiescent") solar X-ray conditions. Following completion of the NEAR mission, Nittler et al. (2001) reported XRS data for five solar flares and two quiescent Sun integrations. These authors used more refined analysis methods than those of the preliminary report by Trombka et al. and included an extensive analysis of systematic errors. Their derived ratios of Mg/Si, Al/Si, S/Si, Ca/Si and Fe/Si are given in Table 1, together with typical

Table 1. Abundance ratios for Eros determined from X-ray and gamma-ray spectroscopy compared to ratios for ordinary chondrites, eucrites, diogenites and pallasites. The latter three groups formed by extensive differentiation of their parent asteroids.

Abundance Ratio[1]	XRS[2]	GRS[3]	Ordinary Chondrites[4]	Eucrites[4]	Diogenites[4]	Pallasites[4]
Mg/Si	0.85±0.11	0.75	0.80	0.14 –0.45	0.5–0.7	1.2–1.5
Al/Si	0.068±0.022	–	0.064	0.15–0.43	0.01–0.07	~0
S/Si	<0.05	–	0.11	0.0–0.05	0.0–0.02	0.01–1.4
Ca/Si	0.077±0.006	–	0.071	0.18–0.38	0.02–0.10	0.01
Fe/Si	1.65±0.27	0.80	1.0 (LL) 1.2 (L) 1.6 (H)	0.4–0.8	0.4–0.6	2.4–18
Fe/O	–	0.28	0.5–0.8	0.2–0.4	0.28–0.36	1–8
Si/O	–	0.61	0.5	0.5	0.5	0.4
K (wt. %)	–	0.07	0.08	0.006–0.08	0.0–0.03	~0

[1]By weight
[2]Nittler et al., 2001, one-sigma errors
[3]Assumed uncertainties are 40% (Evans et al., 2001)
[4]Average compositions and/or ranges taken from a database of literature values (Nittler et al., 2000)

ratios observed in some classes of meteorites. The potassium abundance and ratios of Mg/Si, Fe/Si, Si/O and Fe/O derived from GRS data taken on the surface of Eros have been reported by Evans et al. (2001) and are also given in Table 1. As discussed below, the GRS data agree in some respects with the XRS results but disagree sharply in others. Despite the rather large uncertainties, a number of important results are evident in the data with implications for the history of Eros and its relationship to meteorite samples studied on Earth.

The Mg/Si ratio of Eros determined by the NEAR XRS is 0.85 ± 0.11 (Fig. 15). The one-sigma error bar includes possible heterogeneity on the surface of the asteroid. The GRS value for the landing site (0.75 ± 0.3) is completely compatible with the x-ray result, giving confidence in the derived value. This ratio is essentially identical to that measured in ordinary chondrites as well as that of some other primitive meteorites. This result alone indicates that Eros has not been globally differentiated into a core, mantle and crust. Differentiation strongly fractionates both Mg and Si from their original abundances. For example, eucrites, diogenites and angrites (as well as most crustal terrestrial and lunar rocks) all have Mg/Si ratios lower than ordinary chondrites whereas ureilites and lodranites (residues of partial melting) and pallasites (mixtures of olivine and metal) typically have higher Mg/Si ratios. Some differentiated meteorites are compatible with the observed Mg/Si ratio at the limits of the error bars, but can be ruled out as Eros analogs by other derived element ratios.

The Al/Si and Ca/Si ratios of Eros are both ~0.07, based on XRS measurements (Fig. 16, Table 1). Again, these results are closely similar to those measured in ordinary chondrites and strongly argue that Eros is undifferentiated. Basaltic meteorites (e.g., eucrites) have strongly enhanced Al/Si and Ca/Si ratios, compared to chondrites, whereas other differentiated meteorites have significantly lower ratios (e.g., diogenites, ureilites). We note that both the derived Al/Si and Ca/Si ratios are subject to important systematic

errors (Nittler et al. 2001), but the major source of uncertainty for each ratio is different. Thus, the consistency of these ratios both with each other and with primitive, chondritic compositions is encouraging in that it would appear that the total uncertainty is not significantly larger than reported.

The potassium abundance of Eros, determined from γ-ray emissions from radioactive decay of ^{40}K, is 0.07 ± 0.03 wt% (Evans et al. 2001). This value again overlaps the abundances measured in primitive meteorites, including ordinary chondrites. As with Mg/Si, Al/Si and Ca/Si this result argues against Eros having been globally differentiated. However, K is not as diagnostic an element of differentiation (for example some eucrites have concentrations up to 0.08 wt%) and the large uncertainty in the derived K abundance does not rule out some loss of K from the asteroid's surface.

Perhaps the most surprising result from the NEAR XRS experiment is the discovery that the surface of Eros is strongly depleted in sulfur (Fig. 17) (Trombka et al. 2000; Nittler et al. 2001). The S/Si ratios derived from individual flares vary but all are significantly lower than those measured in bulk chondrites. Because the average value for five measurements is within one sigma of zero, Nittler et al. (2001) reported a two-sigma upper limit on the S/Si ratio of 0.05, a factor of two lower than the average value measured in ordinary chondrites. Nittler et al. discussed three possible explanations for the low S/Si ratio: that Eros formed from S-depleted chondritic material, that Eros has undergone a limited amount of partial melting and melt segregation, or that interaction of the asteroid's surface with the space environment has resulted in loss of S (space weathering). The first explanation is highly unlikely, given the lack of observed primitive materials with low S/Si ratios (including meteorites and interplanetary dust particles). The other explanations deserve further discussion.

The first partial melt to form as a rock of chondritic composition is heated contains ~85 wt.% FeS or ~30 wt.% S (Kullerud 1963). Thus, limited partial melting of a chondritic asteroid and removal of the S-rich melt could produce substantial S depletions. It is clear from the meteoritic record that some asteroids have undergone various levels of partial melting and melt segregation ("primitive achondrites"; Mittlefehldt et al. 1998). For example, acapulcoites have clearly been melted and recrystallized but retain a bulk chondritic composition, indicating little loss of partial melts, while the related lodranites are clearly residues of partial melting and have low S/Si ratios. However, Nittler et al. (2001) pointed out that all known meteorites with low S/Si ratios also show evidence for loss of silicate partial melts (e.g., fractionated Mg/Si and/or Al/Si ratios) not observed on Eros. Also, as argued by McCoy et al. (2000), partially-differentiated asteroids might be expected to show large spatial heterogeneity in their mineralogy and chemical composition. Such heterogeneity was not observed on Eros, but mixing in the asteroid's regolith could in principle homogenize the surface.

Nittler et al. (2001) favored a space weathering explanation for the low observed S/Si ratio. Interactions of charged particles (for example, galactic cosmic rays or solar wind ions), radiation, and micrometeorites with an asteroid's surface would be expected to modify the surface. If such processes vaporize iron sulfides at the surface, S could be lost due to its high volatility. Preliminary calculations of S loss during photosputtering, ion-sputtering and impact vaporization indicate that all of the S present at the surface of a chondritic asteroid could be lost in ten million years. Space weathering is thus a plausible explanation for the low observed S abundance. Further calculations to determine expected effects of space weathering on other elemental abundances are highly desirable.

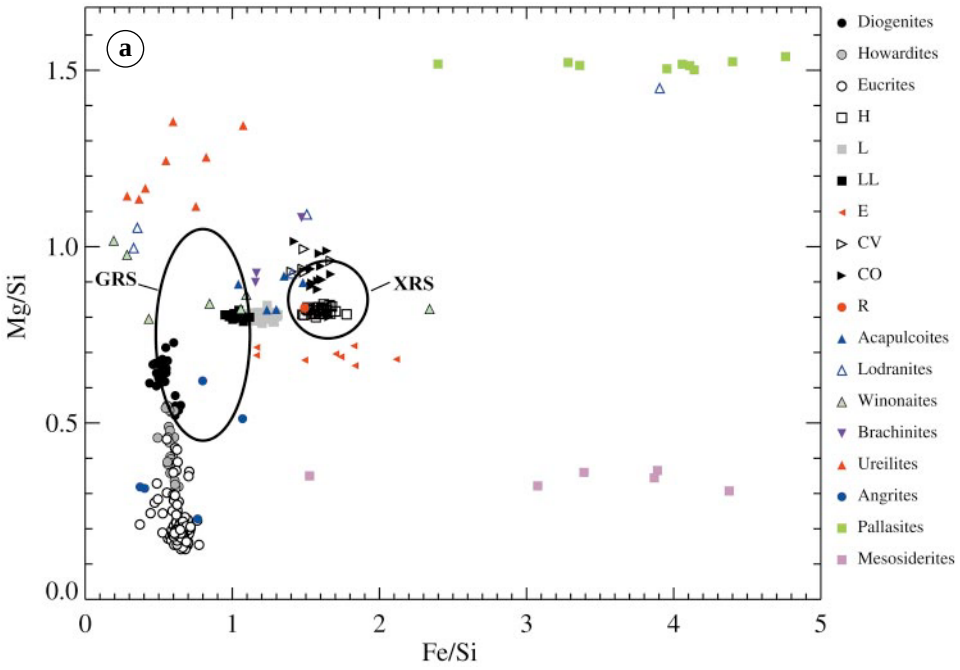
a
GRS
XRS
Mg/Si
Fe/Si
0.0
0.5
1.0
1.5
0
1
2
3
4
5
Diogenites
Howardites
Eucrites
H
L
LL
E
CV
CO
R
Acapulcoites
Lodranites
Winonaites
Brachinites
Ureilites
Angrites
Pallasites
Mesosiderites

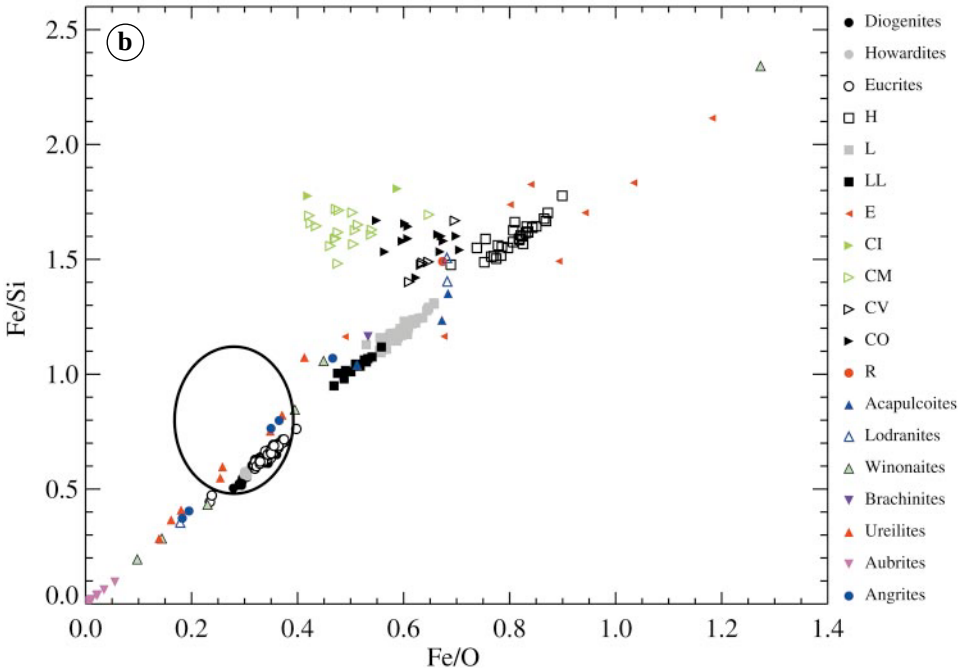
b
Fe/Si
Fe/O
0.0
0.5
1.0
1.5
2.0
2.5
0.0
0.2
0.4
0.6
0.8
1.0
1.2
1.4
Diogenites
Howardites
Eucrites
H
L
LL
E
CI
CM
CV
CO
R
Acapulcoites
Lodranites
Winonaites
Brachinites
Ureilites
Aubrites
Angrites

In particular, potassium is also volatile but does not appear to be depleted on Eros (see above). This could reflect the fact that the GRS experiment samples material at lower depths than the XRS (and GRS only measured one small spot on the surface). We would also note that studies of gas-rich regolith breccias, which sample the upper layer of ancient asteroidal regolith, are an ideal target for future petrologic and chemical studies to determine the extent and nature of S volatilization.

In comparison to the elements discussed above, iron data from NEAR present a much more difficult case to interpret (Fig. 18). The Fe/Si ratio derived by the XRS is 1.65 ± 0.27 whereas that derived by the GRS is significantly different: 0.8 ± 0.3. The XRS Fe/Si value is in good agreement with H- and L-type ordinary chondrites, R chondrites and some other primitive meteorites. In contrast, the GRS Fe/Si is lower than average values for ordinary chondrites (1.0–1.6), although it does overlap LL-type ordinary chondrites within the stated error bar. Additionally, the Fe/O ratio determined by the GRS measurements is 0.28 ± 0.11, also lower than all ordinary chondrites (0.5–0.8).

Evans et al. (2001) discussed possible explanations for the apparent discrepancy in XRS- and GRS-derived Fe/Si ratios, including errors in the XRS and/or GRS results, that Eros is partially differentiated, or that regolith processes have lowered the iron abundance at the NEAR landing site, relative to the bulk surface of the asteroid. These authors considered the first two explanations to be unlikely and favored the third. A significant fraction of iron in ordinary chondrites is in the form of metal, which has very different material properties than the silicates that make up the bulk of the rocks. It is quite plausible that physical processes within an asteroid's regolith could segregate metal from silicates resulting in heterogeneous iron abundances on spatial scales that would depend on the details of the processes. In fact, the low Fe/Si and Fe/O ratios measured by the GRS are consistent with a chondritic composition which has had its metal component removed (Evans et al. 2001). It is believed that the NEAR landing site was within a smooth "ponded" deposit (Veverka et al. 2001b) and Robinson et al. (2001) have suggested that these deposits are preferentially composed of fine-grained material, perhaps segregated by photoelectric-induced dust levitation. This suggestion is consistent with the remotely-sensed abundance ratios. In this case, the physical separation actually removes the silicates from the host rock, leaving a metal-enriched residual material.

The question of metal-silicate segregation in Eros' regolith goes deeper than resolving discrepancies between the X-ray and gamma-ray measurements, however. Regolith processes may well segregate materials as a function of depth, due to size-sorting effects like the "Brazil-nut problem," wherein large grains rise to the surface of a shaken mixture of different sized spheres (Rosato et al. 1987). Fe-Ni metal is both denser and more ductile than silicates and may well have a larger grain size in the regoliths of chondritic

◀ **Fig. 18.** Evidence for metal and sulfide separation is apparent in (a) plot of Mg/Si and Fe/Si weight ratios determined by the X-ray spectrometer and the gamma-ray spectrometer (error ellipses are the 2σ uncertainty for XRS and an assumed 40% error for GRS) and (b) Fe/Si and Fe/O for the gamma-ray derived composition. The low Fe/Si and Fe/O ratios in the gamma-ray derived composition are consistent with removal of Fe-rich (but Si- and O-free) metal and sulfide from a silicate matrix with lesser Fe and significant Si and O.
[Reproduced from Evans et al. (2001) Elemental composition from gamma-ray spectroscopy of the NEAR-Shoemaker landing site on 433 Eros. Meteoritics and Planetary Science 36, 1639–1660.]

asteroids. As discussed by Nittler et al. (2001), without a detailed understanding of these processes, it is probably not possible to determine whether the surface iron abundance determined by remote-sensing is representative of the bulk asteroid.

Mineralogical-chemical synthesis

NEAR's X-ray/gamma-ray spectrometers and multi-spectral imager/near-infrared spectrometer instrument packages gave complementary information on the chemistry and mineralogy, respectively, of the target asteroid 433 Eros. Synthesis of these two data sets provides information not available from either alone, including the abundance of non-mafic silicates, metal and sulfide minerals. McCoy et al. (2001) utilized four approaches to integrating these data sets, including Venn diagrams, normalized element distributions, normative calculations and matrix inversion. The latter two techniques failed to yield useful information. Normative calculations require knowledge of sodium abundance and higher precision oxygen data than were available, while the matrix inversion techniques produced consistent but non-unique solutions. We briefly discuss the results of the Venn diagrams and normalized element distribution techniques.

Venn diagrams provide a useful tool for comparing the properties of two sets of information and determining areas of overlap. In this case, we populate our Venn diagram (Fig. 19) with groups of meteorites permissible as analogs for Eros on the basis of, respectively, the MSI/NIS and XGRS data sets. A wide range of meteorite types are excluded by both the XGRS and MSI/NIS data sets and appear on the diagram outside of the two circles. The XGRS data alone would allow R chondrites and several groups of primitive achondrites (e.g., acapulcoites, lodranites, winonaites, brachinites), but spectra for these groups are a poor match to Eros as determined by the MSI/NIS experiments. In contrast, ureilites and CO chondrites are allowed by the MSI/NIS data, but are poor compositional matches to Eros. The only groups that appear possible on the basis of both data sets are ordinary chondrites that experienced alteration ("space weathering") at their surface or primitive achondrites formed from an ordinary chondrite precursor (i.e., primitive achondrites not yet sampled in our meteorite collections). Differentiating between these two alternatives does not seem possible, although surface alteration of a chondritic body is consistent with evidence from the MSI imaging of extensive surface alteration and regolith formation and movement.

Normalized elemental distributions shed further light on the nature of the alteration. These calculations confirm that it is possible to reconcile the X-ray-derived composition, gamma-ray-derived composition and MSI/NIS-derived mineralogy by incorporating a common silicate mineral abundance and composition with varying amounts of metal and sulfide, consistent with inferences from the XGRS experiment.

Conclusions and epilogue

Without question, the NEAR mission has been a milestone in our study of asteroids and their relationship to meteorites. From an engineering point of view, NEAR achieved a wide array of firsts, including operating further from the sun than any other solar-powered spacecraft, orbiting an asteroid, landing on an asteroid, performing the first

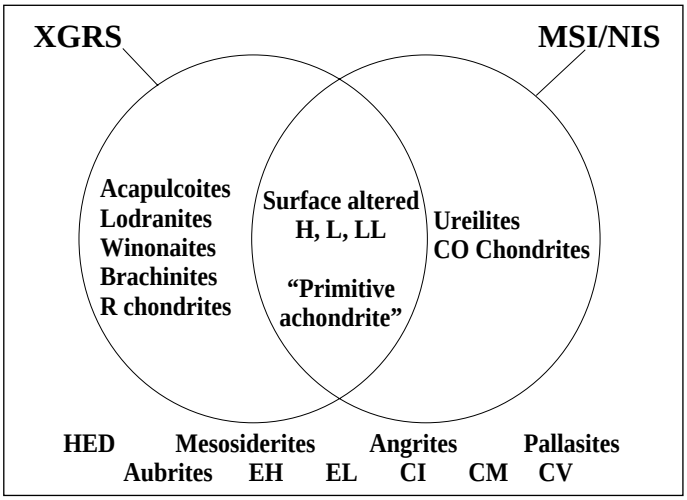

Fig. 19. Venn diagram for the XGRS and MSI/NIS data sets. Those meteorites included in the box but outside the circles are prohibited by both data sets. Those in a circle but outside the intersection are allowed by one data set but not the other. The most likely meteoritics analogs to 433 Eros appear to be H, L, LL or CO chondrites which have been altered at the surface of the asteroid or a type of primitive achondrite derived from a precursor with a mineralogy similar to these chondrites. [Reproduced from McCoy et al. (2001) The compostion of 433 Eros: A mineralogical chemical synthesis. Meteoritics and Planetary Science 36, 1661–1672.]

science on the surface of a small solar system body and, not least of all, recovering from a near-fatal loss of the mission to successfully achieve its scientific goals. From a scientific point of view, NEAR fully achieved its stated scientific objectives (Cheng et al. 1997) of characterizing Eros' physical and geological properties and inferring its elemental and mineralogical composition, clarifying the relationship between asteroids, comets and meteorites, and advancing our understanding of processes and conditions during the formation and early evolution of the planets. Some of the results of the NEAR mission may have been predictable, such as proving that asteroids are geologically more complex than previously envisioned. Others were unexpected, such as providing both spectral and chemical evidence which point to complex processes occurring in the regolith of asteroids or providing our first centimeter-scale images of an asteroid which proved that the surface of an asteroid can present areas with benign landing sights for future exploration. NEAR also provided a blueprint for the future of asteroid exploration. While sample return may ultimately be necessary to answer many of the questions we have about asteroids, we are only beginning our exploration of the diverse group of small bodies that make up the asteroid belt. More than a dozen different types of asteroids exist and basic questions about the diversity within a single type, the full range of geologic processes that operated during their formation and the extent of heterogeneity on a single asteroid remain unanswered. These questions are best answered not by a single sample return mission, but by a fleet of missions that will explore the range of asteroid types. Finally, NEAR points to the geologic diversity that can occur on a single asteroid and the necessity of using global geological, mineralogical and chemical studies as part of any sample return mission to ensure that we sample the full range of diversity on any one asteroid.

Acknowledgements

The science reported here was the culmination of nearly a decade of work by hundreds of engineers, scientists and support technicians working on the NEAR mission. The authors gratefully acknowledge these contributions. We also thank NASA for their financial support of both the NEAR mission in general and the scientific work of the authors of this paper in particular.

Figures 3–12 courtesy of NASA and the Johns Hopkins University Applied Physics Laboratory.

References

Acuña MH, Anderson BJ, Russell CT, Wasilewski P, Kletetshka G, Zanetti L, Omidi N (2002) NEAR magnetic field observations at 433 Eros: First measurements from the surface of an asteroid. Icarus **155**, 220–228

Adams JB (1974) Visible and near-infrared diffuse reflectance spectra of pyroxenes as applied to remote sensing of solid objects in the solar system. J Geophys Res **87**, 4829–4836

Barnouin-Jha O, Cheng AF, Prockter LM, Murchie S, Zuber M, Smith D, Neumann G, Garvin J, Robinson M, Veverka J, Thomas P (2000) Characterizing the regolith of 433 Eros from laser altimeter and imaging. Eos Transactions **81**, F803.

Bell JF, Davis DR, Hartmann WK, Gaffey MJ (1989) Asteroids: The big picture. In: Asteroids II, Binzel RP, Gehrels T, Matthews MS (Eds). Univ. of Arizona Press, Tucson, 921–945

Bell JF III, Izenberg NI, Lucey PG, Clark BE, Peterson C, Gaffey MJ, Joseph J, Carcich B, Harch A, Bell ME, Warren J, Martin PD, McFadden LA, Wellnitz D, Murchie S, Winter M, Veverka, J, Thomas P, Robinson MS, Malin M, Cheng A (2002) Near-IR reflectance spectroscopy of 433 Eros from the NIS instrument on the NEAR mission. 1. Low phase angle observations. Icarus **155**, 119–144

Burke JG (1986) Cosmic Debris: Meteorites in History. Univ. of California Press, pp. 445

Burns RG (1970) Crystal field spectra and evidence of cation ordering in olivine minerals. Am Min **55**, 1608–1631

Burns RG (1993) Mineralogical Applications of Crystal Field Theory (2nd Ed.). Cambridge University Press, Cambridge, England, pp. 551

Bussey DBJ, Robinson MS, Edwards K, Thomas PC, Joseph J, Murchie S, Veverka J, Harch AP (2002) Eros global basemap from NEAR Shoemaker MSI images. Icarus **155**, 38–50

Chapman CR, Merline WJ, Thomas PC, Joseph J, Cheng AF, Izenberg N (2002) Impact history of Eros: Craters and boulders. Icarus **155**, 104–118

Cheng AF, Farquhar RW, Gold RE, Heeres KJ, Ladnshof JA, Lee SC, Santo AG (1997) Near Earth Asteroid Rendezvous: Mission overview. Space Science Reviews **82**, 3–29

Cheng AF, Barnouin-Jha O, Zuber MT, Veverka J, Smith DE, Neumann GA, Robinson M, Thomas P, Garvin JB, Murchie S, Chapman C, Prockter L (2001) Laser altimetry of small-scale features on 433 Eros from NEAR-Shoemaker. Science **292,** 488–491

Cheng AF, Barnouin-Jha O, Prockter L, Zuber MT, Neumann G, Smith DE, Garvin J, Robinson M, Veverka J, Thomas P (2002) Small-scale topography of 433 Eros from laser altimetry and imaging. Icarus **155**, 51–74

Chladni EFF (1794) Über den Ursprung der von Pallas gefundenen und anderer ihr ähnlicher Eisenmassen. Hartknoch, Riga, Latvia. Pp. 63

Cintala MJ, McBride KM (1995) Block distributions on the lunar surface: A comparison between measurements obtained from surface and orbital photography. LPSC **XXV**, 261–262

Clark BE, Lucey P, Helfenstein P, Bell JF III, Peterson C, Veverka J, McConnochie T, Robinson MS, Bussey B, Murchie SL, Izenberg NI, Chapman CR (2001) Space weathering on Eros: Constraints from albedo and spectral measurements of Psyche crater. Meteoritics & Planetary Science **36**, 1617–1637

Cloutis EA, Gaffey MJ, Jackowski TL, Reed KL (1986) Calibration of phase abundance, composition, and particle size distribution for olivine-orthopyroxene mixtures from reflectance spectra. J Geophys Res **91**, 11641–11653

Cole TD, Boies MT, El-Dinary AS, Cheng A, Zuber MT, Smith DE (1997) The Near-Earth Asteroid Rendezvous laser altimeter. Space Science Reviews **82**, 217–254

Evans LG, Starr RD, Brückner J, Reedy RC, Boynton WV, Trombka JI, Goldsten JO, Masarik J, Nittler LR, McCoy TJ (2001) Elemental composition from gamma-ray spectroscopy of the NEAR-Shoemaker landing site on 433 Eros. Meteoritics and Planetary Science **36**, 1639–1660

Gaffey MJ, Bell JF, Brown RH, Burbine TH, Piatek JL, Reed KL, Chaky DA (1993a) Mineralogical variations within the S-type asteroid class. Icarus **106**, 573–602

Gaffey MJ, Burbine TH, Binzel RP (1993b) Asteroid spectroscopy: Progress and perspectives. Meteoritics **28**, 161–187

Goldsten JO, McNutt RL Jr, Gold RE, Gary SA, Fiore E, Schneider SE, Hayes JR, Trombka JI, Floyd SR, Boynton WV, Bailey S, Brückner J, Squyres SW, Evans LG, Clark PE, Starr R (1997) The X-ray/gamma-ray spectrometer on the Near Earth Asteroid Rendezvous mission. Space Science Reviews **82**, 169–216

Hapke BW (2001) Space weathering from Mercury to the asteroid belt. J Geophys Res **106**, 10039–10073

Hawkins SE III, Darlington EH, Murchie SL, Peacock K, Harris TJ, Hersman CB, Elko MJ, Prendergast DT, Ballard BW, Gold RE, Veverka J, Robinson MS (1997) Multi-spectral imager on the Near Earth Asteroid Rendezvous mission. Space Science Reviews **82**, 31–100

Izenberg N, Anderson B (1998) NEAR swings by Earth en route to Eros. Eos Trans. AGU **79**, 289 and 294–295

Kivelson MG, Bargatze LF, Khurana KK, Southwood DJ, Walker RJ, Coleman PJ Jr (1993) Magnetic field signatures near Galileo's closest approach to Gaspra. Science **271**, 331–334

Kullerud G (1963) The Fe-Ni-S system. Ann Rep Geophys Res **67**, 4055–4061

Lee SW, Thomas P, Ververka J (1986) Phobos, Deimos, and the moon – Size and distribution of crater ejecta blocks. Icarus **68**, 77–86

Lee P (1996) Dust levitation on asteroids. Icarus **124**, 181–194

Lohr DA, Zanetti LJ, Anderson BJ, Poterma TA, Hayes JR, Gold RE, Henshaw RM, Mobley FF, Holland DB, Acuña MH, Scheifele JL (1997) NEAR magnetic field investigation, instrumentation, spacecraft magnetics and data access. Space Science Reviews **82**, 255–281

Marvin U (1996) Ernst Florens Friedrich Chladni (1756–1827) and the origins of modern meteorite research. Meteoritics and Planetary Science **31**, 545–588

McCoy TJ, Nittler LR, Burbine TH, Trombka JI, Clark PE, Murphy ME (2000) Anatomy of a partially-differentiated asteroid: A "NEAR"-sighted view of acapulcoites and lodranites. Icarus **148**, 29–36

McCoy TJ, Burbine TH, McFadden LA, Starr RD, Gaffey MJ, Nittler LR, Evans LG, Izenberg N, Lucey P, Trombka JI, Bell JF III, Clark BE, Clark PE, Squyres SW, Chapman CR, Boynton WV, Veverka J (2001) The composition of 433 Eros: A mineralogical-chemical synthesis. Meteoritics and Planetary Science **36**, 1661–1672

McFadden LA, Wellnitz DD, Schnaubelt MW, Gaffey MJ, Bell JF III, Izenberg N, Chapman CR (2001) Mineralogical interpretation of reflectance spectra of Eros from NEAR NIS low phase flyby. Meteoritics & Planetary Science **36**,1711–1726

McSween HY Jr, Bennett ME III, Jarosewich E (1991) The mineralogy of ordinary chondrites and implications for asteroid spectrophotometry. Icarus **90**, 107–116

Mittlefehldt DW, McCoy TJ, Goodrich CA, Kracher A (1998) Non-chondritic meteorites from asteroidal bodies. In: Planetary Materials, Papike JJ (Ed). Reviews in Mineralogy, Vol. **36**, 4–1–195

Morden SJ, Collinson DW (1992) The implications of the magnetism of ordinary chondrite meteorites. Earth Planet Sci Lett **109**, 185–204

Murchie SL, Pieters CM (1996) Spectral properties and rotational spectral heterogeneity of 433 Eros J Geophys Res **101**, 2201–2214

Murchie S, Robinson MS, Hawkins SE III, Harch A, Helfenstein P, Thomas P, Peacock K, Darlington EH, Gold R, Clark B, Bell JF III, Merline W, Izenberg N, Veverka J (1999) Inflight Calibration of the NEAR Multispectral Imager. Icarus **140**, 66–91

Murchie S, Robinson M, Clark B, Li H, Thomas P, Joseph J, Bussey B, Domingue D, Veverka J, Izenberg N, Chapman C (2002) Color variations on Eros from NEAR multispectral imaging. Icarus **155**, in press.

Nittler LR, Starr RD, Lim L, McCoy TJ, Burbine TH, Reedy RC, Trombka JI, Gorenstein P, Squyres SW, Boynton WV, McClanahan TP, Bhangoo JS, Clark PE, Murphy ME, Killen R (2001) X-ray fluorescence measurements of the surface elemental composition of asteroid 433 Eros. Meteoritics and Planetary Science **36**, 1673–1695

Oberbeck VR, Quaide WL (1967) Estimated thickness of a fragmental surface layer of Oceanus Procellarum. Journal of Geophysical Research **72**, 4697–4704

Oberbeck VR, Quaide WL (1968) Genetic implications of lunar regolith thickness variations. Icarus **9**, 446–465

Oberst J, Mottola S, di Martino M, Hicks M, Buratti B, Soderblom L, Thomas N (2001) A model for rotation and shape of asteroid 9969 Braille from ground-based observations and images obtained during the Deep Space 1 (DS1) flyby. Icarus **153**, 16–23

Pieters CM, Taylor LA, Noble SK, Keller LP, Hapke B, Morris RV, Allen CC, McKay DS, Wentworth S (2000) Space weathering on airless bodies: Resolving a mystery with lunar samples. Meteoritics & Planetary Science **35**, 1101–1107

Pike RJ (1977) Apparent depth/apparent diameter relation for lunar craters. In: Lunar Science Conference 8th, 3427–3436

Prockter L, Thomas P, Robinson M, Joseph J, Milne A, Bussey B, Veverka J, Cheng A (2002) Surface expressions of structural features on Eros. Icarus **155**, 75–93

Quaide WL, Oberbeck VR (1968) Thickness determinations of the lunar surface layer from lunar impact craters. Journal of Geophysical Research **73**, 5247–5270

Richter I, Brinza DE, Cassel M, Glassmeier K-H, Kuhnke F, Musmann G, Othmer C, Schwingenschuh K, Tsurutani BT (2001) First direct magnetic field measurements of an asteroidal magnetic field: DS1 at Braille. Geophys Res Lett **28**, 1913–1916

Robinson MS, Thomas PC, Veverka J, Murchie SL, Carcich B (2001) The nature of ponded deposits on Eros. Nature **413**, 396–400

Robinson MS, Bussey DBJ, Edmonds J, Lutsey J, Milne A, Moore K, Prockter L, Wilcox B (2002a) NEAR MSI mosaics of 433 Eros, In: Lunar and Planetary Science **XXXIII**, Abstract #1671, Lunar and Planetary Institute, Houston (CD-ROM)

Robinson MS, Veverka J, Thomas P, Wilcox B (2002b) Geology of 433 Eros., in preparation

Rosato A, Strandburg KJ, Prinz F, Swendsen RH (1987) Why the Brazil nuts are on top: Size segregation of particulate matter by shaking. Phys Rev Lett **58**, 1038–1040

Russell CT (1997) The Near Earth Asteroid Rendezvous Mission. Kluwer Academic Publishers , 308 pp

Santo A, Lee S, Gold R (1995) NEAR spacecraft and instrumentation. J Astronaut Sci **43**, 373–398

Sasaki S, Nakamura K, Hamabe Y, Kurahashi E, Hiroi T (2001) Production of iron nanoparticles by laser irradiation in a simulation of lunar-like space weathering. Nature **410**, 555–557

Schultz PH, Gault DE (1975) Seismic effects from major basin formations on the moon and Mercury. The Moon **12**, 159–177

Thomas PC, Veverka J, Sullivan R, Simonelli DP, Malin MC, Caplinger M, Hartmann WK, James PB (2000) Phobos: Regolith and ejecta blocks investigated with Mars Orbiter Camera images Journal of Geophysical Research **105**, 15091–15106

Thomas PC, Veverka J, Robinson MS, Murchie SL (2001) Shoemaker Crater: A major source of ejecta on asteroid 433 Eros. Nature **413**, 394–396

Thomas PC, Joseph J, Carcich B, Veverka J, Clark BE, Bell JF III, Byrd AW, Chromko R, Robinson M, Murchie S, Procter L, Cheng A, Izenberg N, Malin M, Chapman C, McFadden LA, Kirk R, Gaffey M, Lucey PG (2002) Eros: Shape, topography, and slope processes. Icarus **155**, 18–37

Trombka JI, Squyres SW, Brückner J, Boynton WV, Reedy RC, McCoy TJ, Gorenstein P, Evans LG, Arnold JR, Starr RD, Nittler LR, Murphy ME, Mikheeva I, McNutt RL Jr, McClanahan TP, McCartney E, Goldsten JO, Gold RE, Floyd SR, Clark PE, Burbine TH, Bhangoo JS, Bailey SH, Petaev M (2000) The elemental composition of asteroid 433 Eros: Results of the NEAR-Shoemaker X-ray spectrometer. Science **289**, 2101–2105

Trombka JI, Nittler LR, Starr RD, Evans LG, McCoy TJ, Boynton WV, Burbine TH, Brückner J, Gorenstein P, Squyres SW, Reedy RC, Goldsten JO, Lim L, Hurley K, Clark PE, Floyd SR, McClanahan TP, McCartney E, Branscomb J, Bhangoo JS, Mikheeva I, Murphy M.E (2001) The NEAR-Shoemaker XGRS experiment: Overview and lessons learned. Meteoritics and Planetary Science **36**, 1605–1616

Veverka J, Thomas P, Harch A, Clark B, Bell JF III, Carcich B, Joseph J, Chapman C, Merline W, Robinson M, Malin M, McFadden LA, Murchie S, Hawkins SE III, Farquhar R, Izenberg N, Cheng A (1997) NEAR's Flyby of 253 Mathilde: Images of a C Asteroid. Science **278**, 2109–2114

Veverka J, Thomas P, Harch A, Clark B, Bell JF III, Carcich B, Joseph J, Murchie S, Izenberg N, Chapman C, Merline W, Malin M, McFadden L, Robinson M (1999) NEAR Encounter with Asteroid 253 Mathilde: Overview. Icarus **140**, 3–16

Veverka J, Robinson MS, Thomas P, Murchie S, Bell JF III, Izenberg N, Chapman C, Harch A, Bell M, Carcich B, Cheng A, Clark B, Domingue D, Dunham D, Farquhar R, Gaffey MJ, Hawkins E, Joseph J, Kirk R, Li H, Lucey P, Malin P, Martin M, McFadden L, Merline WJ, Miller JK, Owen WM Jr, Peterson C, Prockter L, Warren J, Wellnitz D, Williams BG, Yeomans DK (2000) NEAR at Eros: Imaging and spectral results. Science **289**, 2088–2097

Veverka J, Thomas PC, Robinson M, Murchie S, Chapman C, Bell M, Harch A, Merline WJ, Bell JF III, Bussey B, Carcich B, Cheng A, Clark B, Domingue D, Dunham D, Farquhar R, Gaffey MJ, Hawkins E, Izenberg N, Joseph J, Kirk R, Li H, Lucey P, Malin M, McFadden L, Miller JK, Owen WM Jr, Peterson C, Prockter L, Warren J, Wellnitz D, Williams BG, Yeomans DK (2001a) Imaging of small-scale features on 433 Eros From NEAR: Evidence for a complex regolith, Science **292**, 484–488

Veverka J, Farquhar B, Robinson M, Thomas P, Murchie S, Harch A, Antreasian PG, Chesley SR, Miller JK, Owen WM Jr, Williams BG, Yeomans D, Dunham D, Heyler G, Holdridge M, Nelson RL, Whittenburg KE,

Ray JC, Carcich B, Cheng A, Chapman C, Bell JF III, Bell M, Bussey B, Clark B, Domingue D, Gaffey MJ, Hawkins E, Izenberg N, Joseph J, Kirk R, Lucey P, Malin M, McFadden L, Merline WJ, Peterson C, Prockter L, Warren J, Wellnitz D (2001b) NEAR Shoemaker's descent to Eros: Unexpected depositional and erosional features in the regolith. Nature **413**, 390–393

Warren JW, Peacock K, Darlington EH, Murchie SL, Oden SF, Hayes JR, Bell JF III, Krein SJ, Mastandrea A (1997) Near infrared spectrometer for the Near Earth Asteroid Rendezvous mission. Space Science Reviews **82**, 101–167

Wetherill GW, Chapman CR (1988) Asteroids and meteorites. In: Meteorites and the Early Solar System, Kerridge JF, Matthews MS (Eds). Univ. of Arizona Press, Tucson, pp. 35–67

Wilkison SL, Robinson MS, Thomas PC, Veverka J, McCoy TJ, Murchie SL, Prockter LM, Yeomans DK (2002) An estimate of Eros's porosity and implications for internal structure. Icarus **155**, 94–103

Yeomans DK, Antreasian PG, Barriot J-P, Chesley SR, Dunham DW, Farquhar RW, Giorgini JD, Helfrich CE, Konopliv AS, McAdams JV, Miller JK, Owen WM, Scheeres DJ, Thomas PC, Veverka J, Williams BG (2000) Radio science results during the NEAR-Shoemaker spacecraft rendezvous with Eros. Science **289**, 2085–2088

Zuber MT, Smith DE, Cheng AF, Garvin JB, Aharonson O, Cole TD, Dunn PJ, Guo Y, Lemoine FG, Neumann GA, Rowlands DD, Torrence MH (2000) The shape of 433 Eros from the NEAR-Shoemaker Laser rangefinder. Science **289**, 2097–2101